Politecnico di Milano

Scuola di Ingegneria Industriale e dell'Informazione
Course of Materials Engineering and Nanotechnology

Design and evaluation of a Tensile configuration for an Impact-testing set-up

Relatore: Prof. Frassine Roberto
Correlatore: Dr. Caimmi Francesco

Mainini Luca (770987)

AA. 2012/13

CONTENTS

LIST OF FIGURES

LIST OF TABLES

Abstract

Il presente documento riassume il lavoro fatto per sviluppare un primo prototipo di un set-up sperimentale. Verrà usato per la valutazione della tenacità dei materiali a veloctà moderate (superiori ad 1 m/s). Il nuovo set-up implementa una prova di impatto a trazione, la ragione di ciò sono due lavori precedenti in cui è stato mostrato come tale configurazione possa agevolare misure di forza in condizioni non quasi-statiche. Tale sistema è stato progettato, realizzato e valutato. La valutazione è stata fatta confrontando il risultati ottemuti con quelli generati usando un'altra macchina, ritenuta affidabile sulla base di anni di sperimentazione. I risultati hanno evidenziato una grande differenza nel comportamento dinamico; tale differenza si è dimostrata limitate per il nuovo set-up. Nonstante forti effetti dinamici siano presenti nelle tracce registrate con il nuovo set-up è stato possibile ottenere dei risultati confrontabili per quanto riguarda la misura della tenacità di PMMA, sia in temini di valore medio che in termini di dipendenza dal parametro a/W. L'ultima parte del report è dedicata alla valutazione di un'ipotesi che potrebbe spiegare perché il set-up sia tanto sensibile agli effetti dinamici: questi effetti sono sempre associati a masse, rigidezze e le interazione tra i vari componenti a contatto e non. Tale studio non si è dimostrato conclusivo e lascia aperta la domanda sul nuovo set-up; ulteriori sviluppi del prototipo dovranno essere basati su un dettagliato studio delle interazioni dinamiche dei componenti, specialemte quelli che connettono il provino alla cella di carico.

The present repost expose the work done to develop a new set-up for impact testing of materials at moderately high speed (above 1 m/s). The new set-up allows force measures in tensile configuration; the choice of this is justified by previous works demonstrating how this approach can be helpful in measuring material toughness. The new set-up has been designed and assembled. In order to check and validate the behaviour of the tool a set of tensile tests were performed; the results were compared with others obtained on a machine (a swing pendulum). It's shown how different are the behaviours of these machines: the reason for this is suspected to lie into the assembly which hold the specimen and the force transducer. This hypothesis has been investigated using an analogue model and ended up with the verification that the stiffness of the whole machine cannot be the reason for so clear difference. Future steps to improve the new set-up must be based on more detailed, dynamic study of the components of the assembly.

1. INTRODUCTION

The present report is the result of the work done in Enschede, Netherlands, by Production Technology group of the Mechanical Engineering Department at the University of Twente. Principal point of the work done aimed to design a new set-up for Tensile impact configuration testing. The interest on this kind of tests is raised by results presented in literature showing lower dynamic effects compared to others configurations such as Three Point Bending (3PB). The need for a simple and fast testing procedure to determine material's toughness alighted the importance of verifying such a configuration: instrumented impact testing methods are easily implemented in laboratories and are cost effective solutions but they have strong limitations due to dynamic effects always present during such tests. These limit the accuracy of the test so much that a threshold of impact velocity (v_{imp}) has been setted as low as 1 m/s, velocity significantly lower than that occurring in many real situations.

The present report is on the path of works by Ghezzi [2] and Visser [3]. Analysis of the behaviour of a new set-up is proposed by comparing test results from two types of machines and conditions.

The first chapter outlines some theoretical basics required to understand the problem. Firstly, an introduction will be given on fracture mechanics: an overview of the Linear Elastic Fracture Mechanics theory (LEFM) and some topics from Fracture Dynamics. The last part of Chapter 2 is dedicated to the international recommendations mostly related to toughness measure via impact testing.

Chapter 3 presents the set-up designed to modify a drop-weigh tower to perform impact tests in a tensile configuration. The chapter illustrates the driving parameters that governed the choices and the differences the new configuration present with respect to the Three-Point Bending (3PB)

configuration.

The fourth chapter presents tests performed to verify the behaviour of the new set-up and the eventual confirmation of the tensile configuration as a better choice for toughness measurements.

In the last chapter is presented an analogue model. This has been used to verify some aspects related to the mechanical behaviour of the test machine.

2. FRACTURE MECHANICS BASICS

In the study of the behaviour of materials it has been found that even if the material shows elastic nature, like ceramics that show almost purely linear elastic brittle behaviour, the failure of a component is not only related to the nominal state of stress and the ultimate tensile strength. In some particular cases this simple approach works but in most cases won't, especially when the component has strange shape or is made of a material with non-linear mechanical behaviour. Many cases of unexpected failure denunciated the need of new criteria for structural design. Parallel to the development of theoretical models to describe the fracture behaviour of materials, experimental knowledge has been developed around it. Some techniques have been proposed to analyse the response of the material in quasi-static and dynamics conditions. These techniques are developed from the most famous and old models: those developed by Charpy's and Izod's [4]. Clearly, the development of the two fronts are inseparable and deeply correlated, because of this the chapter is divided into two main sections: the first about the main theoretical results and the second about the experimental measures performed to get compatible data to compare the results in different situations and from different types of experimental set-up.

2.1 Linear Elastic Fracture Mechanics

The goal of Linear Elastic Fracture Mechanics (LEFM) is to describe the nature of a crack into an object loaded in steady state conditions, so without dynamic manifestations. It's the simplest effective theory to approach the crack propagation problem and is based on some fundamental assumptions:

- linear elasticity

- no limitation to the stress in the system
- negligible time dependence

2.1.1 Energetic model

On these assumptions Griffith proposed an energetic criterion to predict the stability of a crack into a system. The idea is an energy balance of the system that has to hold in any state of loading, the balance has been defined in terms of energy variation. The variation of E should be zero because of the conservation principle:

$$\frac{\partial E}{\partial A} = \frac{\partial W_{ext}}{\partial A} + \frac{\partial U_{el}}{\partial A} + \frac{\partial T}{\partial A} + \frac{\partial W_f}{\partial A} = 0 \tag{2.1}$$

where W_{ext} is the work done by the external forces, U_{el} the elastic potential energy, T the kinetic energy and W_f is the work released due to crack expansion. Griffith defined a parameter, the energy release rate G, defined as

$$G = -\frac{\partial W_f}{\partial A} = \frac{\partial W_{ext}}{\partial A} + \frac{\partial U_{el}}{\partial A} + \frac{\partial T}{\partial A} = G_C \tag{2.2}$$

G_C is the characteristic limiting rate of energy release rate for a material. Griffith tried to correlate this to the surface energy (roughly speaking $W_f = A \cdot \gamma$ so $G_C = -\gamma$) getting a simple but not effective criterion for failure. The principal problem is that he didn't consider any plastic effect that is almost always present; any way he found some good results for very brittle materials.

Irwin proposed to modify this model introducing a correction factor to the term W_f to take into consideration the presence of plastic deformations

$$W_f = W_{surf} + U_{plast} \tag{2.3}$$

The difference from the curve R and the parameter defined by Griffith is that the first is not a single valued but a function of the notch depth a due to presence of plastic deformations. In Irwin's model we can identify a point on

the curve which correspond to G_C in Griffith's model; that point is identified as ultimate condition that discriminate stability and instability of the crack, it's marked on Figure 2.1b as "instability". Knowing the relation between σ and a, dependent on the geometry of the system and on the loading condition, we can find the point (G_C,a_C) that defines the condition of global instability of the crack: there is no equilibrium beyond this condition. The problem of this approach is that is difficult to estimate the exact value of the dissipated energy by means of plastic deformation. This kind of evaluation requires the knowledge of the state of stress around the crack tip, which is not trivial and is still one of the main challenges in theoretical and computational mechanics.

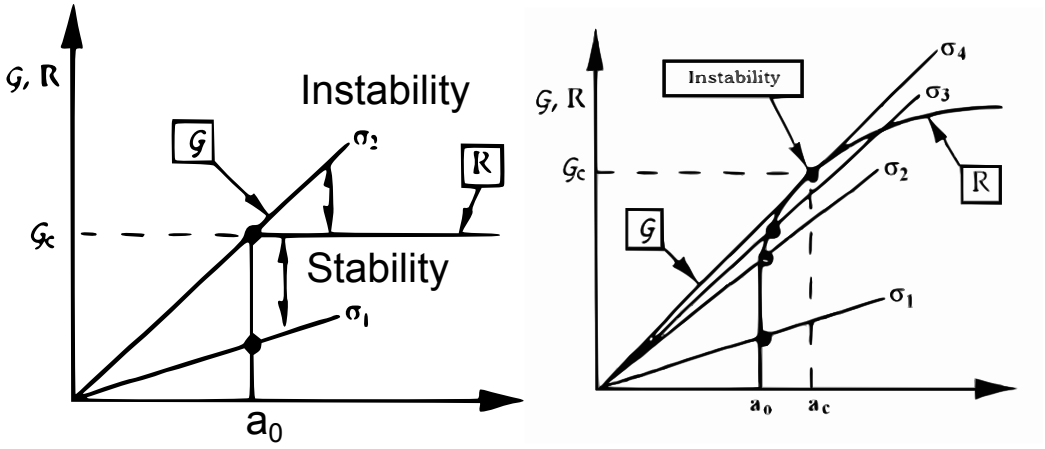

Fig. 2.1: R curve and G_{IC} in the mainframe of LEFM. a) Griffith's model b) Irwin's model

2.1.2 Stress model

Another approach to the fracture problem is the one that Irwin and Westergaard proposed.It's based on the idea that there is a limiting stress state that causes the failure at a certain point, this generates the so called *process zone*. It's an attempt to recover the classical criteria based on the stress condition of a section of a body. These researchers proposed to model the behaviour with

an asymptotic solution near to the crack head and to neglect what happens inside the process zone.

The starting point is the solution that Inglis proposed for the stress field around a elliptical hole in an infinite medium with uniform boundary conditions. It has been found that at the edge of the hole the stress is higher then nominal one

$$\sigma_y = \sigma_n \left(1 + 2\sqrt{\frac{a}{\rho}}\right) \tag{2.4}$$

where a is ellipse's axes in the direction orthogonal to loading and ρ is the curvature radius at the corresponding apex. It's straightforward that the stress is higher for larger cracks as it's proportional to $\sqrt{a}$. On the other side the sharper the discontinuity, the higher the concentration of the stresses which cause the rising of the maximum stress to $\sigma \to \infty$ per $\rho \to 0$. This is physically impossible and here is the main limitation of using this solution.

Westergard and others demonstrated that any asymptotic solution for the mechanical problem have a form that goes with $\frac{1}{\sqrt{r}}$ close to the tip but out of the plastic zone. Westergaard proposed a generalized expression, valid for the three loading modes[1], the form of the solution is

$$\sigma = \frac{K_I}{\sqrt{2\pi r}} f\left(r\right) \tag{2.5}$$

The generality of these solutions is hidden in the term K_I, the stress intensity factor, that depends on problem's geometry: $f(a/W)$, the shape-factor describes this and is unique for any given geometry and is valid only for that only. The stress intensity factor is defined as

$$K_I = \sigma_n \sqrt{2\pi a} f\left(a/W\right) \tag{2.6}$$

where $\sigma_n = \frac{F}{S}$ is the nominal stress, a is the notch depth and $f(a/W)$ is the shape-factor that describes the stress concentration.

[1] In Figure 2.2 are shown the three possible cases of loading for a crack in a plate and in general in a body with a notch.

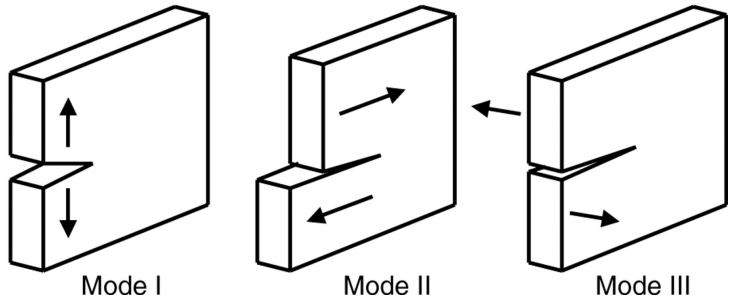

Fig. 2.2: The three modes of loading that can affect a crack or a notch.

Examples of the shape-factor are

$$f(a/w) = 1 + 0.122\cos^2\left(\frac{\pi a}{2W}\right)\sqrt{\frac{2W}{\pi a}\tan\left(\frac{\pi a}{2W}\right)} \qquad (2.7)$$

$$f(a/w) = 1.12 - 0.231\frac{a}{W} + 10.55\left(\frac{a}{W}\right)^2 - 21.72\left(\frac{a}{W}\right)^3 + 30.39\left(\frac{a}{W}\right)^4 \qquad (2.8)$$

respectively for the Double Edge Normal Tensile (DEN(T)) specimen and for the Single Edge Normal Tensile (SEN(T)) specimen. The actual state of stress at the tip of the flaw can be calculated, knowing the geometry and the nominal load. The Stress Intensity Factor is verified against the toughness of the material, K_{IC}: it becomes the new parameter for the failure criteria instead of σ_{yield}. The drawback of this approach is that the shape factor has to be known and this implies solving the elastic problem around the crack. In most cases no analytical solution can be deduced, the consequence is switch to numerical ones that have to be verified and confirmed.

A direct extension of this model is the introduction of a limit to the stress sustainable by the material, considering a yielding stress σ_y we can distinguish two cases: plain stress, for which the maximum stress is σ_y, and plain strain[2], $3\sigma_y$. Forcing the new stress field to sum to the same force as before we get to an expression for the radius of the plastic zone in the two

[2] Imposing $\epsilon_z = \frac{\sigma_z - \nu(\sigma_x + \sigma_y)}{E} = 0$, if $\nu = 0.33$ and $\sigma_x = \sigma_y$ then $\sigma_z = 0.66\sigma_x$.

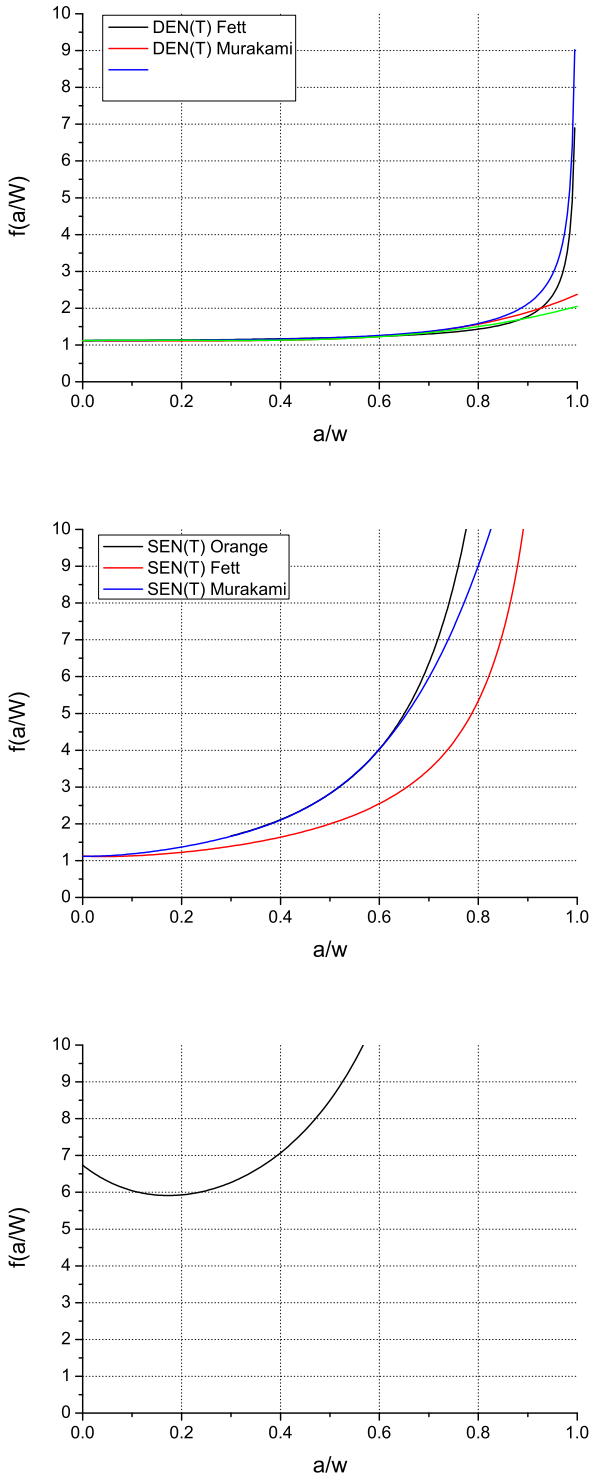

Fig. 2.3: Shape factors. The figures represent the shape factor characteristic of DEN(T), SEN(T) and SEN(B) specimens. On abscissa is plotted a/w and on ordinate is $f(a/w)$.

cases:

$$r_p = \frac{K_I^2}{2\pi\sigma_n^2} \tag{2.9}$$

$$r_p = \frac{K_I^2}{18\pi\sigma_n^2} \tag{2.10}$$

The shape of the plastic zone is obviously not circular but depends on the loading mode and on the dimensions of the component. In Figure 2.4 two approximate shapes of this region are illustrated, in general these are estimated by means of Guest-Tresca or von Mises criteria. In figure 2.5 the difference of the two extreme situations of load close to a notch tip is visualized. A dependence of the toughness on the thickness of the specimen has been identified, this can be easily explain noting that thick specimens have smaller plastic zone, so the thicker the specimen the more fragile it is. In Figure 2.5 the generic dependence of toughness from component thickness is depicted.

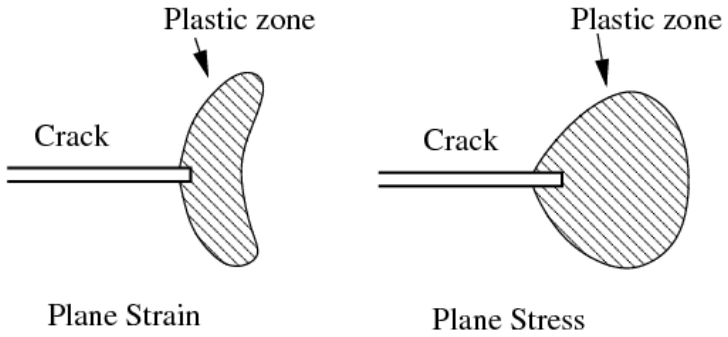

Fig. 2.4: Sketch of the shape of plastic zone in plain-stress and plain-strain conditions.

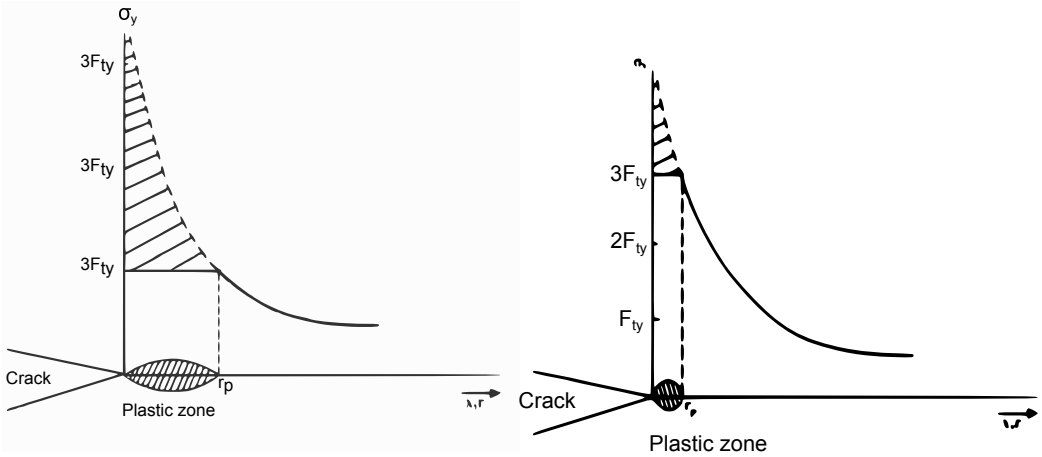

(a) *(b)*

Fig. 2.5: Schematic of the stress field for elastic-perfectly plastic material in case of plain stress condition (a) and plain strain (b)

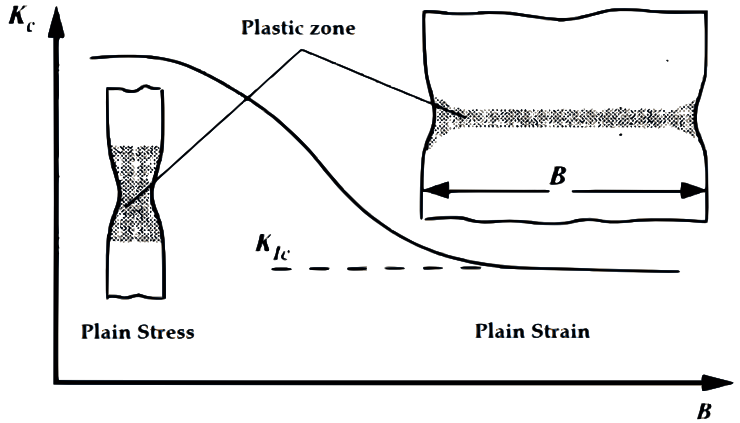

Fig. 2.6: The critical toughness have been found to depend on the thickness of the body and in particular it decreases with growing thickness due to suppression of plastic deformations which absorb energy.

2.2 Fracture dynamics

An other step forward in the level of description is that of the dynamic behaviour of materials: the introduction of time dependence in the elastic problem shows many interesting phenomena that affect sensibly the response of the material to a stimulation of such kind. Some phenomena that help a better understanding of the failure in impact tests will be reported.

2.2.1 Dynamic phenomena

An introduction to this topic is given by considering four papers prepared by Ravi and Knauss [5, 6, 7, 8]. They describe some of the most important phenomena that characterize the dynamic behaviour of material failure in a qualitative manner. They tested Homalite-100 under various rates of loading (up to 10^5 MPa/s) to investigate the dependence between instantaneous stress intensity factor and velocity, as well as initiation toughness and found a relation of K_I with t_f: $K_I - K_{IC} = \frac{const}{t_f^2}$. They also investigated the micro-mechanical process associated with the crack propagation for Homalite-100 and the manifestation of crack branching. In the last paper they investigated the effect of stress waves interaction with the crack: at very high load rates the crack propagates at speeds comparable to that of sound in the material so the stress field on the crack head is no more describable by the average effect of stress waves, it depends on the instantaneous fluctuations.

Another important aspect of dynamic loading is the relation between crack speed on toughness. Arakawa and Mada [9] reported dependence on the instantaneous value of velocity and acceleration. In their research they found that K_{ID} is qualitatively proportional to the velocity, they also found that at a given speed the fracture toughness is higher if reached after deceleration then during acceleration. They also reported the uniqueness of the $K_I^{dyn}(t) - velocity$ relation for acceleration-free cracks. Finally they found that a precise, single-valued relation exists between toughness, velocity and acceleration, so that we can say $K_I^{dyn}(t) = f(v, a)$. This is confirmed by some mathematical solutions of the elastic problem.

This is valid for a moving crack but basically our interest is on the initiation

event: to define a criterion Ravi-Chandar [10], reformulated the quasi-static criterion introducing a rate dependence: the comparison is again between the instantaneous intensity factor K_I^{dyn} determined by an event and the dynamic initiation toughness of the material K_{Id}

$$K_I^{dyn}(t_f) = K_{Id}(T, \dot{K}_I^{dyn}) \tag{2.11}$$

where t_f defines the instant of fracture initiation and T is the temperature. Equation 2.11 clarifies that to determine dynamic fracture toughness experiments in a specific and appropriate range of temperatures and load rates are required.

2.3 Standard tests

2.3.1 Impact testing

The development of fracture mechanics theory is related to the evolution of experimental procedures to measure the Stress Intensity Factors during impact. The aim of all the efforts in this direction is to allow the estimation of the toughness of materials to have an effective design criterion.

There are many aspects that characterise the testing procedures depending on *testing configuration*, *machine's characteristics*, *type of specimen* used and *measured quantities*. The main test configurations are those for *Charpy's* (3PB), *Izod's*, One Point Bending (1PB) and Tensile Impact. In this work two of these have been compared, 3PB and Tensile impact, to collect information about reliability and convenience in using one or the other.

The machines mostly used and known are the *swing pendulum*, *drop-weight tower*, *Hopkinson's bar* (projectile), electro-magnetic devices and servo-hydraulic ones. Any of these are suitable for determined applications depending mainly on the load capacity, the loading rate required and the possibility to use instrumentation. Refer to Table 2.1 to have an idea of their range of applicability.

An other classification key is type of specimen. Basically there are four

	Quasi-static	Drop-weight	Projectile	Explosive	Electro-magnetic
Loading rate $\dot{K}_I^{dyn}(t,v)$ $[MPa\sqrt{m}/s]$	1	10^4	$10^4 - 10^8$	10^5	10^5
Time to fracture t_f $[\mu s]$	$> 10^5$	~ 100	$1 - 100$	$1 - 20$	$10 - 100$

Tab. 2.1: Machine characteristics

main specimen shapes:

- Single Edge Notch (Bending) SEN(B)
- Single Edge Notch (Tensile) SEN(T)
- Double Edge Notch (Tensile) DEN(T)
- Compact Tension CT

The various specimens are applied in many configurations which are all characterized by their own shape factor, as the way of clamping determines the boundary conditions. For a general reference on the form factors consider Rooke [11].

Finally it's possible to discriminate between the technique adopted to measure/estimate K_{Id}. The first tests performed by Charpy and Izod had only the possibility to measure the difference of potential energy before and after the test. With the advent of electronics and proper transducers it has been possible to modify the tests performed introducing measures of the forces exchanged between the striker and the specimen during the impact; this is the case of Instrumented Impact Tests. "Instrumentation" is used when the test is performed with the aid of piezo-electric transducers to capture the forces exchanged between the striker and the specimen. Also measures of displacement have been added to obtain force-displacement plots giving insight about the behaviour and the elastic energy accumulated.

Other techniques have also been developed to measure the state of stress directly, Photo-elasticity and Caustics method are examples of very effective

ways to analyse and measure K_I^{dyn} and so to estimate K_{Id}. Even if these techniques are more accurate then those based on force and displacement measures, they are complex and require sophisticate set-ups. Because of this, the effort in the present research is reasonable, considering that most labs don't have possibility to get those facilities.

2.3.2 Available standards and documentation

This work refers to ISO 8256 [12], ISO 13586 [13] and ISO 17281 [14] standards. In the following the procedure adopted to perform any experiment is presented.

All tests should be performed recording at least the force trace, also displacement records are of interest but not fundamental. If also displacement is recorded it's possible to evaluate the energy associated to the impact directly. The $F - \delta$ curve is compared with the equivalent obtained by integration of the acceleration corresponding to the recorded force: from the second law of dynamics we know that $m_{\mathrm{CM}} a_{\mathrm{CM}} = \sum F^{ext}$ so with double integration the displacement is

$$s(t) = \int_0^t [v_0 - \int_0^{t'} \frac{\sum_{n=1}^{N} F_n^{ext}(\alpha)}{m_{\mathrm{CM}}} d\alpha] dt' \tag{2.12}$$

so

$$s(t) = s_0 + v_0 t - \int_0^t \int_0^{t'} \frac{\sum_{n=1}^{N} F_n^{ext}(\alpha)}{m_{\mathrm{CM}}} d\alpha dt' \tag{2.13}$$

To finalize this calculation the force at any instant is required, as well as the mass of the falling weight and the velocity at contact (v_0), s_0 is actually not interesting since we can set it at zero without loosing meaning on the result. Typical example of the result from impact tests are given in Figure 4.1.

The main estimation of fracture toughness is done using the asymptotic approximation and considering F_Q the force at *fracture initiation*

$$K_Q = K_I^{dyn}(t_f) := \frac{F_Q}{B\sqrt{w}} f(a/w) \tag{2.14}$$

where a is the notch depth, B is the thickness of the specimen, w the width and $f(a/w)$, as always is the shape-factor. If non-linearities are within 5% we can say $F_Q = F(t_f)$; should be noted the difference from the theoretical definition of intensity factor ($K_I = \sigma_n\sqrt{\pi a}f(a/w)$). Considering that the intensity factor always refers to the nominal stress $\sigma_n = \frac{F}{A_n}$ at the notched section a "post mortem" measure is the most comfortable and precise way to estimate the area. Figure 2.7 reproduce the regression method proposed in ISO standards.

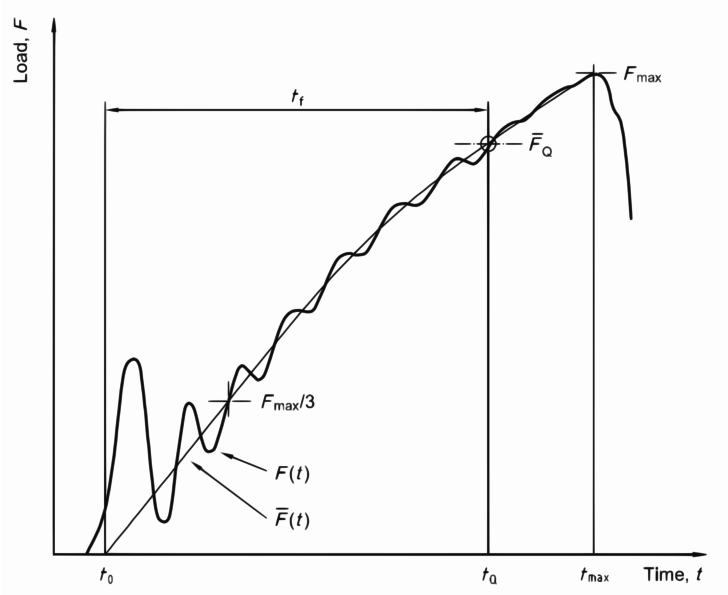

Fig. 2.7: Scheme for the regression method proposed in ISO 17281.

The measure of δ provides an independent estimation of K_{Id} from the one just presented; a first rough indication of the reliability of the result comes from the comparison of the two. To measure the dissipated energy, W_B, during the failure event the curve $F - \delta$ is integrated from t_0 to $t_0 + t_f$. The critical rate of energy release is then

$$G_{Id} = G_Q := \frac{W_B}{Bw\phi(a/w)} \tag{2.15}$$

if the restrictions on the quality of data are fulfilled. $\phi(a/W)$ is the

equivalent of the shape-factor for the energetic procedure[3]. The relation between G_{Id} and K_{Id} is simple in case LEFM is valid:

$$G_{Id} = \frac{K_{Id}^2}{E'} \tag{2.16}$$

with $E' = E$ in plain stress and $E' = \frac{E}{1-\nu^2}$ in plain strain.

Many authors have analysed the dynamic manifestations recognised in the tests. Starting from the experimental approach should be mentioned the work of Aggag and Takahashi [15], who present a general analysis of the effect of filtration on the signals from impact tester. The general conclusion from that work is that the reliability of the estimation of K_Q can be increased properly in this way but careful calibration of the filtration method have to be done. In the same paper mechanical dampers are recognised as more reliable than electronic or digital filtering. A drawback of this method is that to get a precise estimation of the fracture energy we have to compensate energy absorption due to the damper. Figure 2.8 show data presented by Molnàr and al. [16], they have shown the effect of mechanical damping on maximum force and fracture energy. The application of this damping is not always fruitful but in general helps to get better results. Nonetheless some numerical manipulations have been found to be reliable and effective, as shown by Xi [17].

In those cases in which the dynamic effects are too severe other solutions can be adopted: huge efforts have been carried out to define a model to describe oscillating system with spring-damper-mass models. Starting from the early works of Marur, Simha and Nair [18], many authors published models to evaluate the effective force acting at the crack section from the measured one. Examples of this are the publication of Pavan [19], Pettarin, Frontini and Eliçabe [20] and Sahraoui [21]. Other viable solutions are those proposed by Kalthoff and Böhme [22] and Böhme [23]. The main point of their proposal is to reduce the difficulties of achieving a reliable K-history once

[3] In standard ISO 13586 is mentioned $\phi(a/W)$ as a form factor that is specific for the kind of specimen and test configuration. Indications about SEN(B) and CT only are given there.

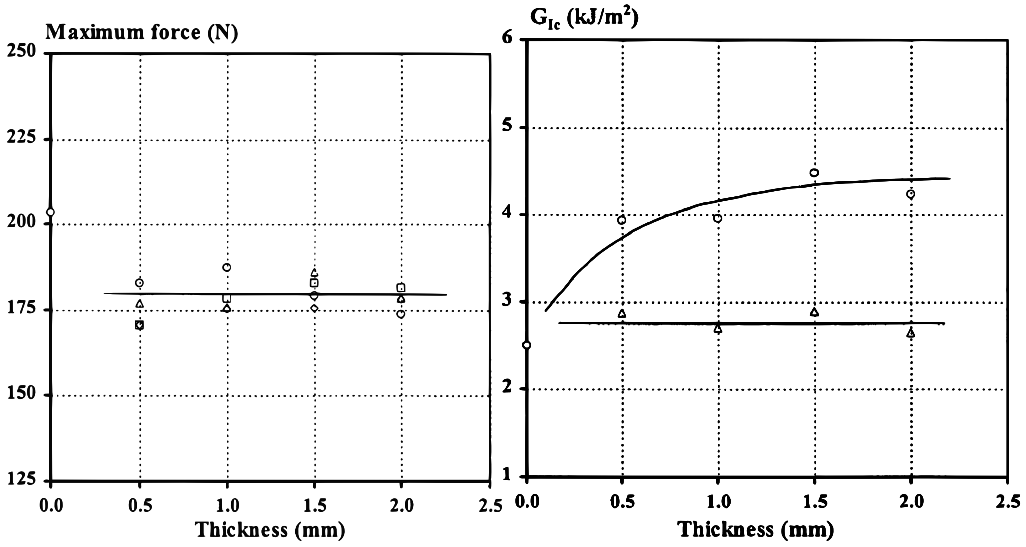

Fig. 2.8: The independence of fracture force from the thickness of the damping layer is quite evident, as well as the non-linear dependence of the fracture energy release rate G. In b) the horizontal line represent the corrected values where the higher one the raw calculated data.

per parameter set. They made the hypothesis that the response has always the same shape and that fracture toughness can be determined knowing just the time to fracture. They defined the dynamic stress intensity factor as

$$K^{dyn}(t) = K^{stat} * k^{dyn}(t) \tag{2.17}$$

$k^{dyn}(t)$ is the dynamic key factor for the test condition, which is determined once by means of adequate techniques, like the caustic method. Once determined, $k^{dyn}(t)$ results in the value of K_{ID} via $K_{ID} = K^{stat} * k^{dyn}(t_f)$. The simplicity of evaluating t_f gives value to this procedure but the limit is in the requirements on key-curve's evaluation: a calibration is required any time a parameter in the test is changed. A further possibility to bypass dynamic effects is to consider the compliance of the specimen and to correlate the displacement, not sensitive to dynamic effects, with the load acting on the specimen; research on this have been done by Khanna [24], Lorriot [25], Parnas and Bilir [26] and Landrien [27]. This last approach is

promising because both displacement and time can be calculated accurately. The disadvantage of this technique is that it relies heavily on the value for the specimen compliance and the difficulty to model this parameter correctly.

3. NEW SET-UP DESIGN

As a matter of fact tensile impact configuration turns out to be a promising choice but still requires further development. The main reason explaining why it has not been analysed deeply before is that historically the Charpy's test is considered adequate in any general condition so there have never been need for new tests. On the other side reasons to choose it dwell in the flexibility of the configuration to different shapes of specimens, higher stability of the interaction between the supporting system, the specimen and the impactor and the damping effect of inertial oscillations produced by the specimen itself due to this viscoelasticity. Another important aspect that favours tensile configuration, not mentioned in the two preceding works, is hidden in the sensitivity of the calculations from the collected data. Ghezzi's master thesis [2] presents the preliminary study of the applicability of standardized methodologies to the new test configuration. He also verified what the real conditions of loading are: broad or very precise informations on the material properties can be found depending on the boundary conditions applied and considered for data analysis. Ghezzi verified that the behaviour of the specimen during the impact is neither rotation-constrained nor rotation-compliant, just a mix of the two. In this situation the definition of proper form factor is critical and difficult. Analytical solutions are not available and numerical solutions require accuracy in describing many aspects of the impact and of constrains their self. This introduces a problem: if the sample is not allowed to rotate freely, in case of asymmetry of the load, of the specimen or of the constrains, a bending momentum will also load the specimen, modifying the state of stress at the crack tip. The second work, by Visser, is the consecutive, more accurate study of the aspects correlated to the new test. It confirms the previously discovered accuracy in evaluating K_Q, even at

speeds of about 3.7 m/s. Vibrations have been recorded in the specimen that can rise doubts on what happens during impact.

3.1 Design drivers

Some fundamental aspects have been chosen as determining drivers for the design process of the set-up: supports' stiffness, components' weight, symmetry, ease of assembly and maintenance, cost and not least the similarity to the corresponding machine used for testing materials[1].

3.1.1 Stiffness and Mass effects

To understand why stiffness and light weight are fundamental issues for this and other machines, it's helpful to consider a mass spring model such as the one represented in Figure 3.1. The second equation of dynamics corresponding to the system represented in Figure 3.1a is

$$m\ddot{x} = -kx \tag{3.1}$$

with the corresponding eigen-frequency

$$\omega = \sqrt{\frac{k}{m}} \tag{3.2}$$

so the higher the stiffness (k) and the lower the mass (m), the higher the resonance frequency. This is of help for the present work as it estranges the possibility to stimulate vibrational modes both for the fixture and the striker. Even in presence of damping phenomena the principle holds true and with reference to the second scheme of Figure 3.1 the resonance frequency in case

[1] CEAST pendulum 6545/000, equipped with a tensile testing fixture, CEAST M 1303 6547.919, and connected to CEAST DAS 8000 data acquisition system. The set-up is setted into the material testing laboratories of the department of Chemistry, Materials and Chemical Engineering of 'Politecnico di Milano', Milan. It consists of a pendulum equipped with an hammer that hits a cross-head fixed which the specimen is fixed.

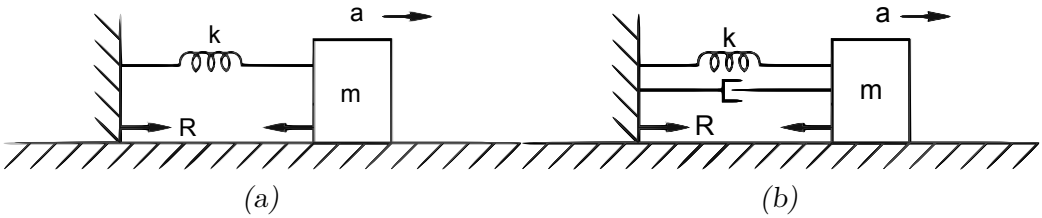

Fig. 3.1: Scheme of a simple oscillator model and of a damped one.

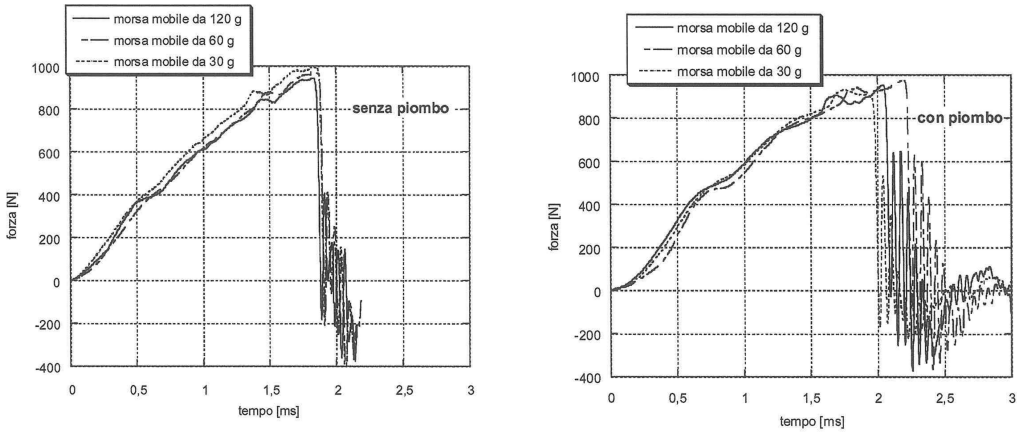

Fig. 3.2: Force traces recorded at 0.5 m/s, $a/w = 0.5$ for three different free cross-heads[2].

of under-damping, which mostly occurs in our case, is

$$\omega = \sqrt{\frac{k}{m} - \left(\frac{\gamma}{2m}\right)^2} \tag{3.3}$$

in this case the mass is still at the denominator and the stiffness at numerator but the frequency is lower because of the second term. Ghezzi analysed the influence of the mass of the clamp on the force traces recorded during tests and found that with increasing the mass the oscillations became stronger even in presence of damping layers. In Figure 3.2 a comparison of some tests to verify this phenomena is shown. A rough idea of $\sqrt{\frac{k}{m}}$ can be calculated considering the oscillations that appear after the fracture initiation: they are representative of the oscillator consisting of clamp and half a specimen. The estimated frequencies are presented in Table 3.1.

Tab. 3.1: Characteristics frequencies of the elements connecting the specimen and the transducer.

	Pendulum	*Drop-weight clamp*	*Drop-weight striker+cross-head*
Mass	3.6 Kg	53 g	4.8 Kg
Stiffness	1 KN/mm	10 KN/mm	100 KN/mm
Frequency	1 Hz	10^4 Hz	$10^4 - 10^8$ Hz

3.1.2 Symmetry

It's important to prevent the occurrence of bending moments. The presence of of such moments indicates the assumptions of pure tractions is violated, it can also introduce a second mode of loading. Tensile tests correspond to a opening mode of the notch but if we bend the specimen in the direction orthogonal to the crack edge we have a more complex stress state. The different loading conditions of the edges causes the uncertainty on the real condition of the stress state at the fracture instant. *The ideal condition to avoid any moment to act on the specimen is to induce the forces to lay exactly on the a line passing through the centre of mass of specimen, cross-head and clamp.* Even if this is one of the most crucial points it has been not exactly fulfilled because of choices for simplicity of production and assembly, especially about the fixed clamp and the free cross-head, they are not fully symmetric but have been drawn such that for the range of thickness's considered (from 2 mm to about 5 mm) the applied force is close to the specimens axes. A solution would have been a self-centring clamp and cross-head composed of two small beams fixed with transversal screws but as a first attempt it seemed uselessly complicated or prone to misalignments errors and vibrations.

3.1.3 Reproducibility

Another issue for the design is to make the new set-up comparable with the existing one, in order to have a term of comparison. Reasonable compatibility

[2] Images taken from Ghezzi[2]

of instruments determined strongly the final result in many aspects. The first similarity is about the use of an *hinge* in between the sample and the frame to reduce the eventual momenta; in the present work have been chosen a multi-axial hinge to try to overcome somehow also both the two bending modes possible. The second common point is the connection of the fixed clamp to the hinge: it's made by a screw that has to react to the force coming from the striker and to compress the force cell. The load cell consist of a piezoelectric ring and is capable to measure only dynamic compressional loads (it's not glued to the clamp), so pre-compression is required to have part of the range of measure in the "tensile" region.

3.2 Components of the machine

The original machine is a drop-weight tower, Dynatup 8200, and it is supposed to be able to perform tests up to a hight of about 2 m with the possibility to change impact energy by changing mass. The same set of masses is available in the modified version but the set-up is heavier and this determines the lowest energy applicable. The differences from the original version lay in the cart itself and in the configuration of the sample holder and striker.

3.2.1 The carriage

The new carriage is composed of two parts, similar and symmetric with respect to the plain defined by the rails. It's made of Aluminium and runs on four air-bearings which reduce friction. The result is a drastic reduction of any mechanical resistance making the loss of energy negligible during the fall and, most important, during impact (during impact other energy dissipations are present and have to be taken into account). Another fundamental improvement determined by this is the reduction of any backlash in the carriage with respect to the rails: the impact point is precisely determined and repeatable.

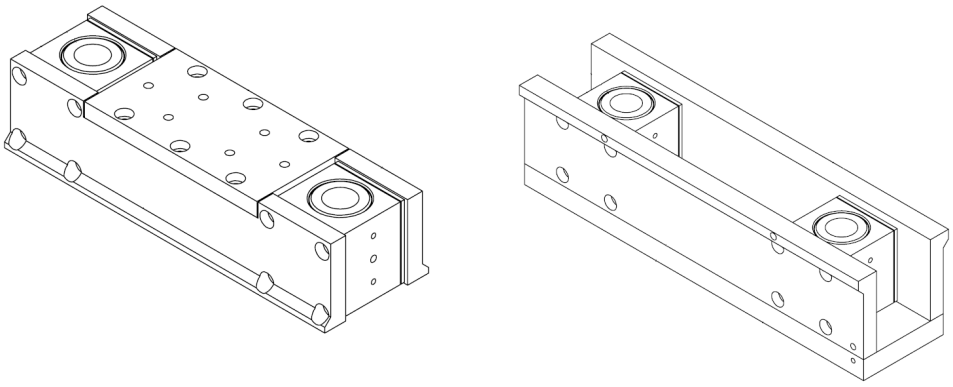

Fig. 3.3: Carriage's schematic drawing.

3.2.2 Fork - impact striker

The impact striker consist of an element with two long legs that permit to reach the free cross-head and to hit it remaining close to the axis of the specimen. It's represented in Figure 3.4. Another fundamental aspect is that it's made such that can hold two force cells at the bottom of the legs, allowing the measure of the actual interaction of the fork with the cross-head. The shape of this part is critical, the presence of the two load cells imposes restrictive conditions on flatness, orientation and position of the surfaces that will host the transducers: eventual misalignments introduce errors and delays in the impact event with the obvious consequences on the experimental results. The precision of the measures are also affected by off-axes forces on the force cell, in fact the presence of it implies non-uniform stresses inside the component and unexpected charges due to the piezoelectric effect; non-uniform stresses are also dangerous for the structural integrity of the cell since this is made of ceramic material and so suffers stress concentrations and point-wise loading situations.

The load cells are all Kistler, type 9001a[3]. The two connected to the fork are used in compression conditions so there are no problems in the positioning of them into place where for the third one the tensile forces applied require a calibration to achieve an optimum condition for the range of measurable loads.

[3] The main characteristics of the load cells are: maximum load 9 kN, maximum bending moment 5 Nm, stiffness ~ 1 kN/μm and sensitivity ~ -4.3 pC/N

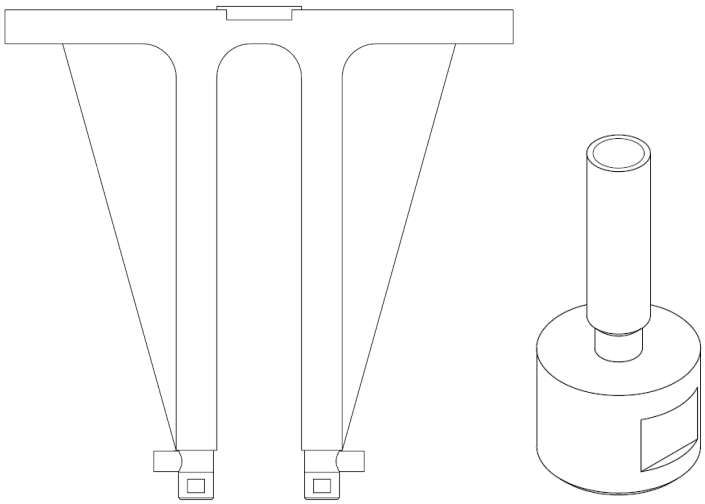

(a) (b)

Fig. 3.4: Striker, load cells and striker's heads.

It requires pre-compression of the transducer: a bolt is tightened on the load cell, the expected maximum load measured is of about 1 kN in tension, so quite far from the limit.

The striker is completed with two elements that have to constitute the contact surface. They are positioned between the load cells and the cross-head and so they are in between the cells and the specimen: any mass in this condition contributes to affect the measure and so introduce "noise" in the acquired data. As a consequence of this Titanium has been chosen instead of Steel because having half elastic modulus and half density of steel it permits to have lighter components but same natural frequency.

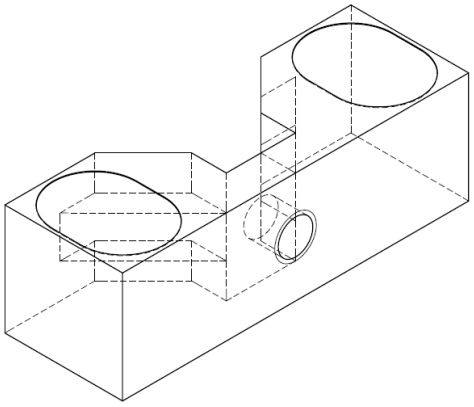

Fig. 3.5: Free cross-head.

3.2.3 Free cross-head

The cross-head is attached to the specimen and is responsible to transfer the load from the striker to the specimen. The importance of this component is also determined by the fact that it is the location where takes place the impact. It's loaded from both the sides and because of this it has to be bending-stiff. Another fundamental aspect is the position of the centre of mass: as said before, it has to be aligned with the centre of mass of the specimen, that of the fixed clamp and of the load cell's one. Due to ease of production and assembly, but also because of the will to test specimens of different thickness, this has not been fulfilled exactly. The distance of the centre of mass varies for any thickness, reaching a minimum for specimens 2 mm thick. The particular shape of this element permits a proper alignment of the two parts that constitute the clamp, the massive part is responsible for guiding the smaller counterpart and to reduce motions and specimen's slipping. The shape also shows tapering to help in reducing mass, in fact also the cross-head is in between the specimen and the sensors; for the same reason Titanium is used also here. A last detail are the embossed areas on the top surface. Finely machined, correspond to the real impact zone and have been embossed to permit a fast application of a 0.1 mm thick layer of grease to give a damping effect.

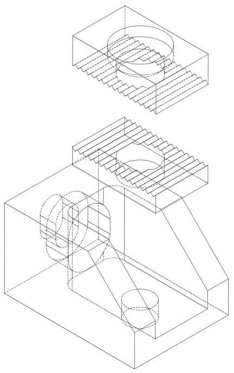

Fig. 3.6: An exploded representation of the three components of the fixed clam.

3.2.4 Fixed clamp

The most complex part of the set-up is the fixed clamp. It holds the specimen and transfer the load from it to the main transducer. Due to the complex shape it's been divided in three parts that are the main component and two plates that constitute the clamping contact surfaces. Force's transmission takes place by friction between a plate and the main component so is important to ascertain that the screw that produces the normal force in the clamping sandwich is sufficiently tightened. To have a rough idea of the amplitude let's consider $\mu_{static} = 0.36$, the calibration of the amplification system used have been done considering a maximum force of 1 kN so it's reasonable to consider this the maximum shear force we want: $F = 1$ KN$= \mu_{static} P$ so P, the load into the screw is $P = \frac{1000}{0.36} = 2.78$ KN.

3.2.5 The hinge

The selection of a proper hinge is fallen on a rod-end that fits properly lightness, size and friction requirements. The selected model is GIKPR5-PW. The only is problem reported until present is a gradual deformation of the low friction ring which results to be too soft: when deformed allow some backlash.

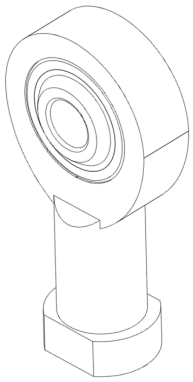

Fig. 3.7: 3D render from the producer of the rod-end, GIKPR5-PW

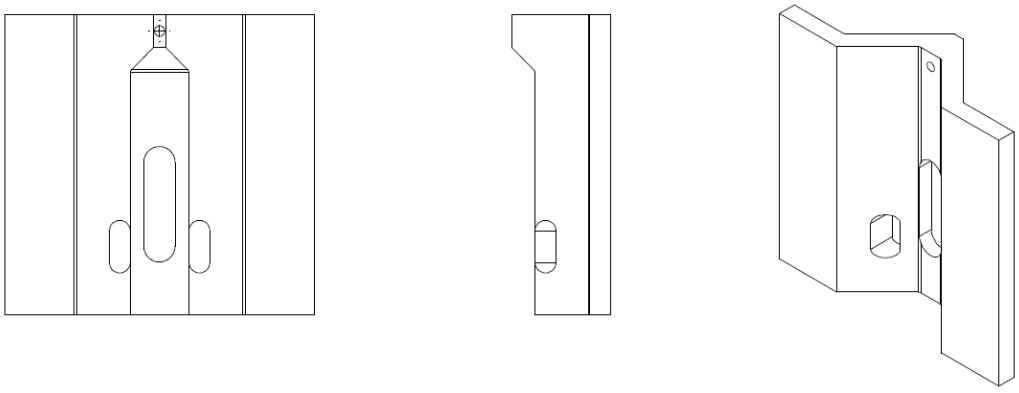

Fig. 3.8: Trigonometric and prospective representations of the frontal leg of the frame.

3.2.6 The frame

The frame supporting the fixed clamp and the specimen itself consists of two vertical elements with a "V" profile that give constrains to a bolt and through this to the inner spherical part of the rod-end. They are anchored to the rest of the machine by a total of six bolts that allow to consider the connection almost as a rigid joint. In the profiles a window have been made to allow a sight of the specimen, at the section of the notch, and of the impact zone on the cross-head. Figure 3.8 shows a heavy design that allows to have a wide space for the specimen and to constrain properly the hinge.

In addition to the exposed compound of elements designed ad hoc the set-up is completed by an high speed camera, a set of force three transducers, a charge amplifier and an acquisition board. An high-speed camera has been used to get direct information about what happens during the impact.

4. TEST RESULTS

The work done in designing the new set-up allowed to have a test machine, which was expected to be capable to perform impact tests in tension. The machine has been scored testing specimens of two kind, SEN(T) and DEN(T), at different speeds and materials. In what follows the results obtained are presented and compared with equivalent ones from the pendulum. To have a wider picture of the behaviour of the machine some three-point bending tests have been done to check where the results in that configuration are comparable with those from other testers. The two configurations have shown some differences: under some aspects the new set-up appears much more sensitive to alignment and to the behaviour of the specimen itself.

From the results obtained, the finding presented by Pavan and Draghi [1] are confirmed. They recognized the pendulum model as a better machine showing compared tests. They presented tests on four kinds of materials (PVC, HDPE, PMMA and RTPMMA) with use of four set-ups: three-point bending on a pendulum and on a drop-weight tower and a one-point bending on the same testers. They have shown that the results are strongly different in the various cases: configurations, materials and impact conditions. In Figure 4.1 and 4.2 some diagrams are shown that give an insight of their results.

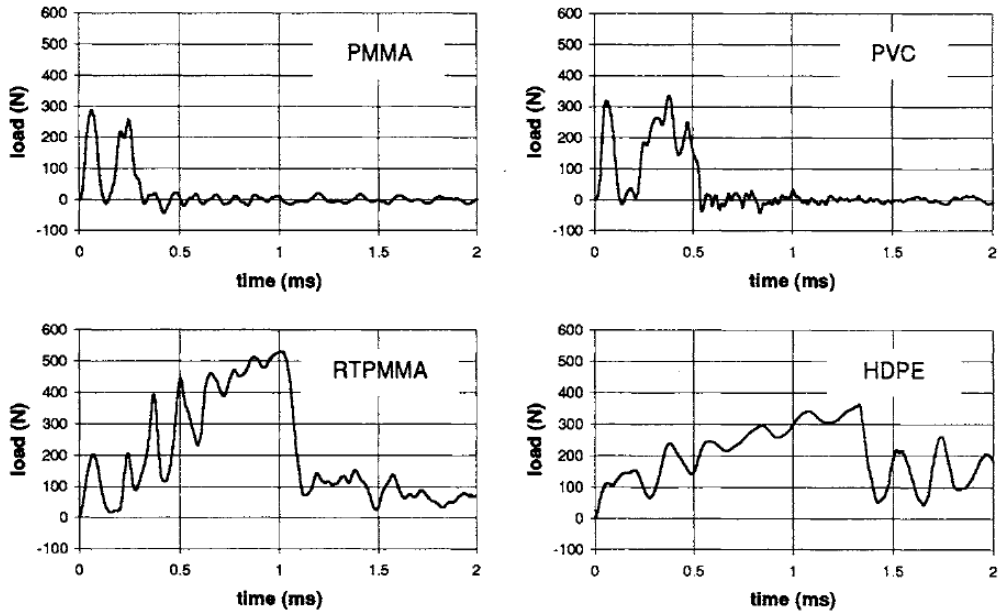

Fig. 4.1: Example of load-time impact curves obtained on different materials. Tester: falling dart, 1 m/s, $a/W = 0.5$. Reproduced from Pavan and Draghi [1].

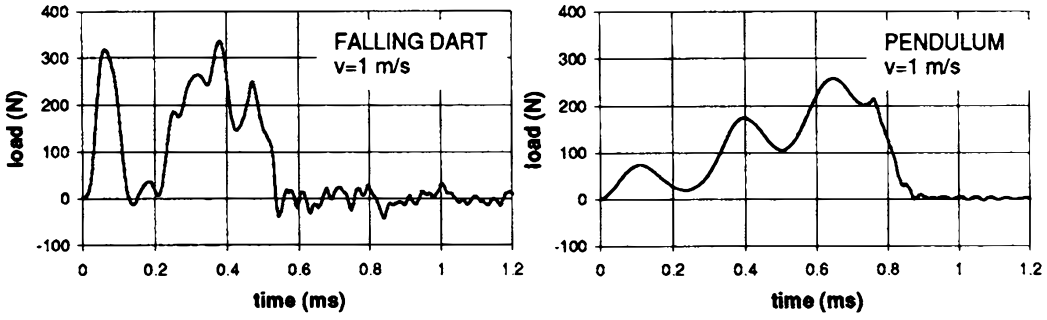

(a) *(b)*

Fig. 4.2: Load-time signals recorded by different testers at impact speed. PVC, a/W= 0.5. Reproduced from Pavan and Draghi [1].

4.1 Specimen preparation

Sample preparation followed the recommendation given in the relevant international standards 13586 [13] and 17281 [14] and by Visser [3]. As reported in these documents the procedure has the aim of producing samples with defined geometry and characteristics that make them adequate to fulfill hypotheses that found the LEFM theory. These characteristics are grossly *homogeneity*, *linearity*, *pure elasticity* (to be precise we should say "dominant" instead of "pure" for the present case).

To prepare the specimens and to avoid the occurrence of non-linear effects, like plasticization, as much as possible the steps are the following:

- machining to the proper dimensions
- production of the notches
- check for defects
- thermal treatments
- conditioning

The machining process can be performed with any machine and technique that allows to introduce as small non-linearities as possible. In the present case all the specimens have been produced on a manual milling machine with the support of air flow cooling. Dimension tolerances are set at 0.02 mm for width and thickness and length by standards but the precision on the specimens used is around 0.1 mm; precision was limited by the milling machine used. Notch depth have to be guaranteed not to vary along the thickness for more than 10%. In Figure 4.3 are represented the two geometries proposed in ISO 13596.

The preparation of the notch is the most critical step because the notch itself makes the specimen weak against the advancing blade: after the blade have been used for two or three notches is opportune to change it or to renew the lateral edges.

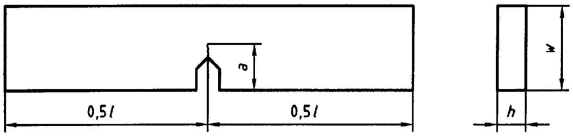

Key

w	Width	
l	Overall length	$l > 4{,}2w$
h	Thickness	$w/4 < h < w/2$
a	Crack length	$0{,}45w < a < 0{,}55w$

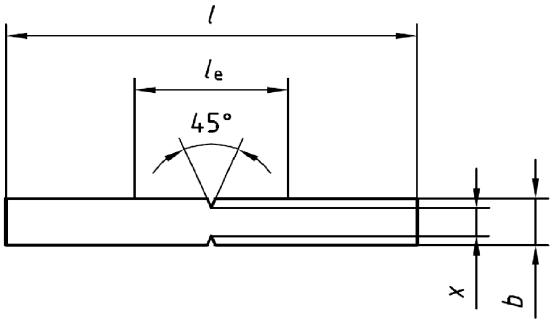

Dimensions in millimetres

Specimen type	Length l	Width b	Preferred value of dimension x	Preferred value of dimension l_0	Free length between grips l_e	Radius of curvature r
1	80 ± 2	10 ± 0,2	6 ± 0,2	—	30 ± 2	—
2	60 ± 2	10 ± 0,2	3 ± 0,2	10 ± 0,2	25 ± 2	10 ± 1
3	80 ± 2	15 ± 0,2	10 ± 0,2	10 ± 0,2	30 ± 2	20 ± 1
4	60 ± 2	10 ± 0,2	3 ± 0,2	—	25 ± 2	15 ± 1
5[a]	80 ± 2	15 ± 0,2	5 ± 0,2	10 ± 0,2	50 ± 2	20 ± 1

[a] For type 5: b' = 23 mm ± 2 mm, r' = 4 mm ± 0,5 mm, l' = 11 mm ± 1 mm.

Fig. 4.3: Three-point-bending (SENB) test specimen with standard restrictions to specifications as in 4.1, ISO-13586:2000.

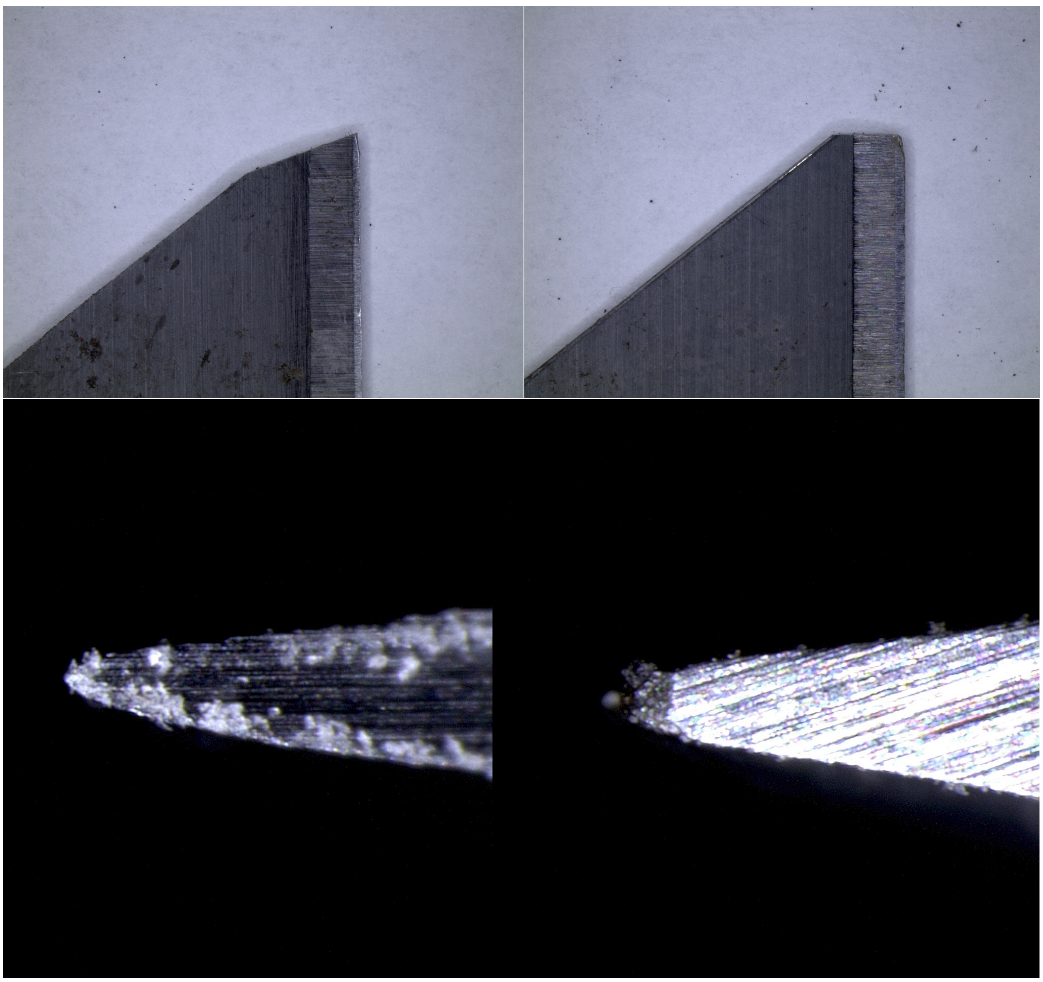

Fig. 4.4: Photos taken with an optical microscope of the two types of blade's tips.

The coarse machining of this step produce residual stresses inside the material altering the final behaviour at failure of the specimen. These are not controllable and so make the specimens not reproducible. To reduce this effect it's made use of the visco-elastic nature of polymers: they have been thermally treated for 30 minutes at $112°$ for PMMA, and at $92°$ for PVC. After this thermal process the specimens are ready to be used if they don't show any defect or deviance from the nature of the material.

4.2 Test procedure

Before proceeding with the exposure of the results obtained it's mandatory to describe the test procedure itself. The set-up preparation, as the disassembly, requires about 20 minutes. Most of the time is spent to prepare and place the high speed camera, which has to be placed carefully to avoid misalignments that affects the focus of the images: the camera used is equipped with an optical system that has very narrow depth of focus. The preparation of the rest of the set-up, so *drop heigh*, *specimen clamping* and finally *placement of the specimen in position*, is much quicker and takes 10-15 minutes if change of velocity of the falling dart is required. After this the test preparation is over. Particular care have to be placed in defining the hight of drop because this is proportional to v_i and, especially for slow impacts, small errors produce quite wide changes in velocity; refer to Appendix B.

Once the height is calibrated, the sensors are checked and the specimens are installed: the specimen, as said before, is held by a clamp connected to the central force transducer and is tightened to the cross-head. Due to the presence of the notches the specimen is extremely weak and can be easily broken before the test. To avoid this problem both cross-head and fixed clam are tightened to the specimen and properly aligned with respect to it by means of a frame that keeps the three parts in place while the assembling procedure is performed (Figure 4.5). Eventually a layer of grease can be applied at the impact zone; the uniformity of the layer is fundamental to guarantee coherence and repeatability of the various tests performed; the presence of a groove of 0.1 mm of depth helps in this procedure. The preparation of the

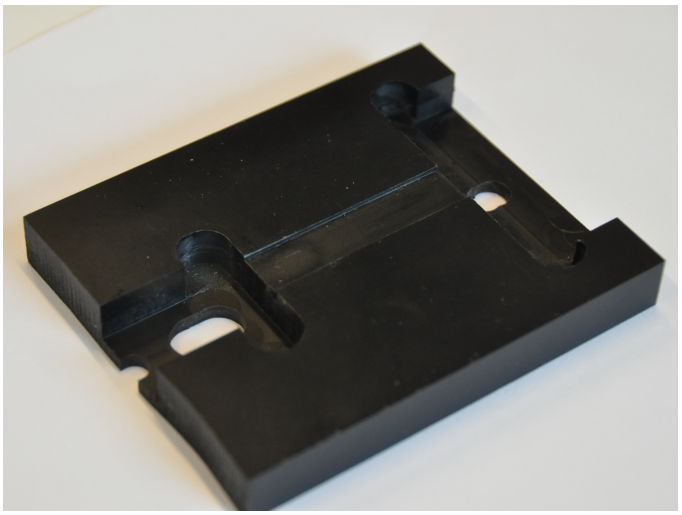

Fig. 4.5: Frame used to fix the clamp and the cross-head to the specimen.

test is concluded when the specimen is in position and aligned.

The most critical part of the test is identified as being the alignment since small errors cause discordance between force traces recorded from the striker. An example of this is presented in Figure 4.11. The less synchronous the two impacts of the fork are, the less reliable the results: in some cases, especially without damping material, the results are unacceptable. Any time the load is not symmetric the specimen fails from one side only. This has also been recognized in the recordings with an high-speed camera where is possible to see the specimen falling and rotating after failure. A block of plastic foam has been prepared, this holds the cross-head in position and makes the test more reproducible.

Signals recorded and recording system

During the test the recorded signals are: *time steps*, form the internal clock of the DAQ electronics, *three force signals* recorded from the force cells trough a charge amplifiers. In addition to the required signals, the displacement of the hammer is recorded by means of an optical trigger, the displacement has a resolution around 0.1 mm.

The completion of the data set is done collecting size' measures of the

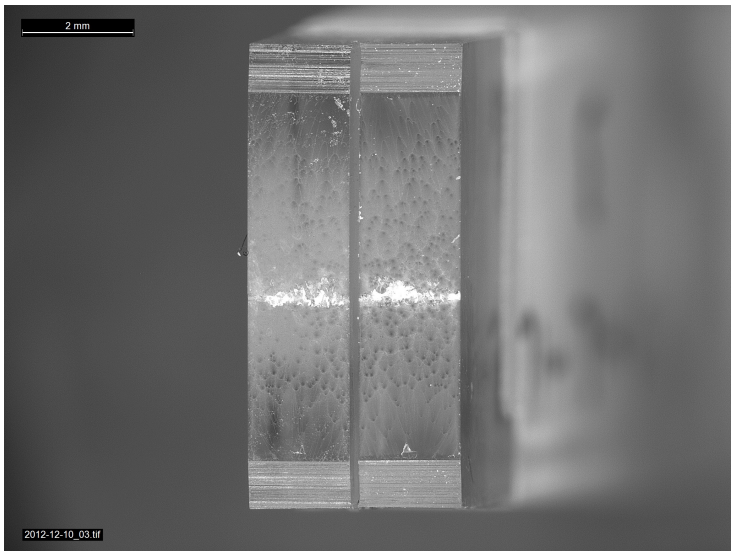

Fig. 4.6: Example of specimen that present both notches as source of cracks propagating, the central white line corresponds to the merging point of the to cracks.

specimens. Normally these geometrical measures are performed after the test itself so that they can all be done at the highest precision. In the present work the geometrical parameters are collected performing measures on calibrated images taken on stereo microscope; in case of DEN(T) specimens the depth of notch of interest if the one corresponding to the side from where the crack is grown. A correct test should show both cracks growing, good tests are possible also with the new set-up and since those are characterized by a nearly synchronous run of the two crack fronts, the measures of both the notches are required and the deepest notch has to be considered in the calculations.

4.3 Test performed

The experimental part of the present work can be divided in two main sections: a first set of tests to study the drop tower (both 3PB and tensile configurations) and a second on the pendulum set-up. In the following the set of test performed will be presented and subsequently the results obtained will be discussed.

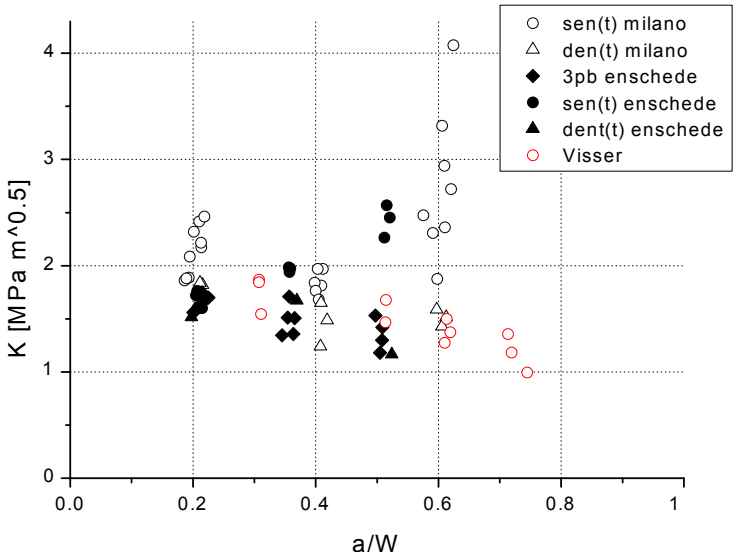

Fig. 4.7: $K_Q - \frac{a}{w}$. Fracture toughness for PMMA, $v_{imp} = 1$ m/s. The curve should be horizontal in case of perfect correspondence between model and experiments.

4.3.1 Enschede. 3PB configuration

Before starting to test the specimens with the new set-up some three-point bending tests have been done. Purpose of this is to give a comparison reference from the same machine: the 3PB tests have been performed following the standards. Therefore these measurements can be expected to be reliable, if valid according to the standards. These test, performed without damping, show too wide oscillations to comply to standards' requirements. Nonetheless linearisation method allowed to calculate values of toughness in agreement with those form Visser [3]. The calculated toughness values are in good agreement with those proposed by Visser in an internal report and in the corresponding publication [3].

The set of specimens consist of fifteen plates of PMMA with nominal thickness 5 mm, width 10 mm, and a span of 40 mm against a length of 42 mm. The chosen depths of notch are the same used for other tests performed in Enschede. The recorded forces are those reproduced in Figure 4.8, 4.9 and 4.10.

Analysing data, a measure of material's toughness have been obtained

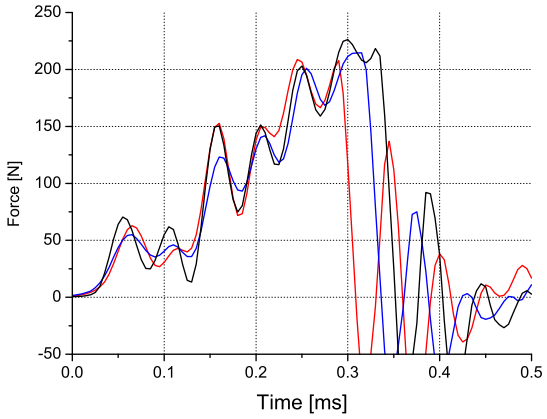

Fig. 4.8: PMMA, SEN(B), $a/W = 0.2$ $B = 5$ mm. $v_i = 1$ m/s.

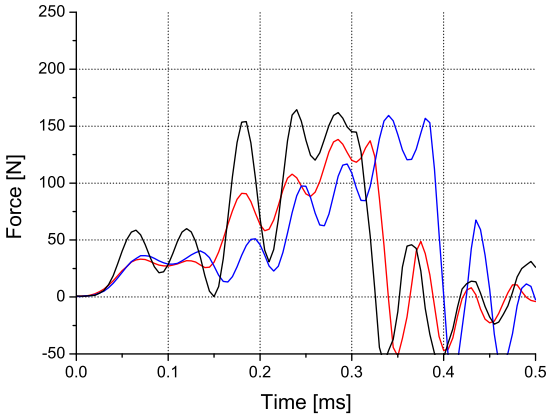

Fig. 4.9: PMMA, SEN(B), $a/W = 0.35$ $B = 5$ mm. $v_i = 1$ m/s.

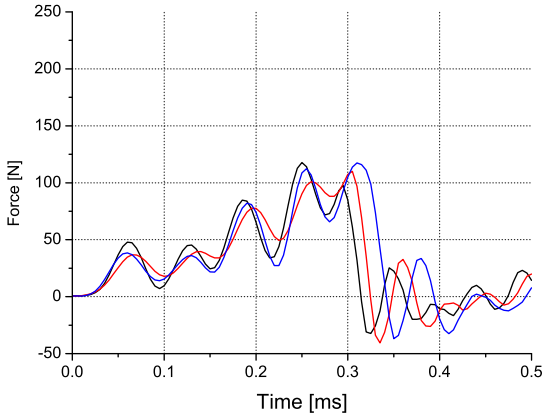

Fig. 4.10: PMMA, SEN(B), $a/W = 0.5$ $B = 5$ mm. $v_i = 1$ m/s.

and it appears to correspond to the tests performed in Milan with the tensile configuration set-up; the gross value is about 2 MPa$\sqrt{m}$ but it's possible to verify that the point-wise value is decreasing with the growth of a in agreement with known data. Direct verification of this can be done looking at Figure 4.7. The agreement of results with data do not disregard the adequacy of the machine chosen for testing toughness of polymeric materials at moderate velocities. It also demonstrates that if the test is performed in proper conditions (linearity and elasticity conditions are respected) the presence of oscillations is not a limit to the test that can be regressed by means of the procedure proposed by the standard.

4.3.2 Enschede. Preliminary tests for tensile configuration

Purpose of the preliminary tests performed is to understand what happens to the specimen and to the set-up in the most common testing conditions. The use of a material, PMMA, instead of other materials is been driven by the amount of raw material available; with that some DEN(T)* samples[1] have been prepared. They are different from those prepared following the ISO indications but are still quite similar to the standard ones. The main differences are in the notch shape (the sharpness of the edge) and in the thermal treatments: in these specimens no thermal relaxation of the eventual stresses have been considered. From these preliminary tests the importance of a proper alignment it's been identified; another aspect that has been recognized is the possible presence of multiple inertial peaks for the lateral traces: the presence of different separate peaks is symptomatic of loss of contact between the fork tips (the strikers) and the cross-head (the anvil). The problem that comes with this is that during the experiment the loading condition of the sample changes, if this is true one of the base conditions is not met and the test must be considered not valid nor reliable. The identification of loss of contact is easy and can be done checking the lateral traces looking for null or negative forces after the first peak. Refer again to Figure 4.11 for

[1] Asterisk is used here to indicate the mentioned specimens have a geometry different from that proposed by the standards

an example. It's useful notice how the dynamic behaviour in the two traces changes: the one recorded downstream of the specimen presents no inertial peak while the ones upstream do; the first show oscillations after the fracture propagation but these fluctuations are not present in the lateral traces.

In any test performed an initial force rise of the trace can be recognized. In any test this kind of oscillations is present and makes the regression never compliant to the requirements of linearity. The height of this first oscillation depends strongly on specimen's thickness. The background of this behaviour has been studied using specimens with deep notches (weak samples): in these cases plastic deformations seem to occur with a non-linear rise of the force. Nonetheless signals' analysis showed that the maximum force is higher than that expected at fracture for weak specimens. For specimens with notch depth $a/W = 0.5$ the forces were almost the same for $a/W = 0.35$ specimens where the time to fracture are a bit lower: considering the case of DEN(T) specimens with 2 mm thickness the forces are about 40 N and time ranges from 0.2 ms to 0.25 ms. The problems rising with this dynamic behaviour is that it masks the real force signal which is of interest here. The origin of this problem is recognized to lie in the dynamic nature of the test and is related to the inertia of the set-up. Verification of this conclusion can be obtained considering the different situations encountered and comparing them: the parameters that mostly affect the dynamic behaviour are masses and stiffness's, so different cases have been considered. Ad hoc specimens have been tested to have further indications: to check the effect of stiffness, an un-notched specimen made of Carbon Fibre Reinforced Polymer (CFRP) have been used. The result of the test is shown in Figure 4.13. In the same figure other traces for specimens with different stiffness's are reproduced, in the legend are mentioned in order of decreasing stiffness. The change of amplitude is related to the dynamic behaviour of the system and increases with the stiffness of the specimen. Another aspect alight by this comparison is that increasing the stiffness of the specimen the recorded traces tend to show increasing steepness.

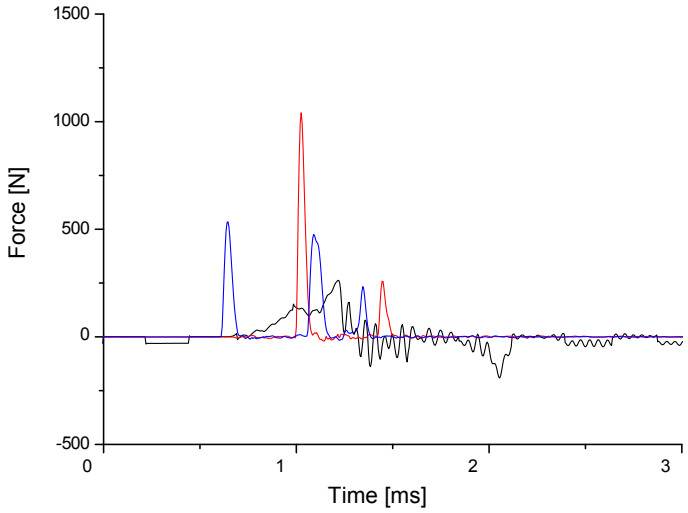

Fig. 4.11: PMMA, preliminary test, DEN(T)*. The three traces correspond to the three transducers: central (black), right (red) and left (blue).

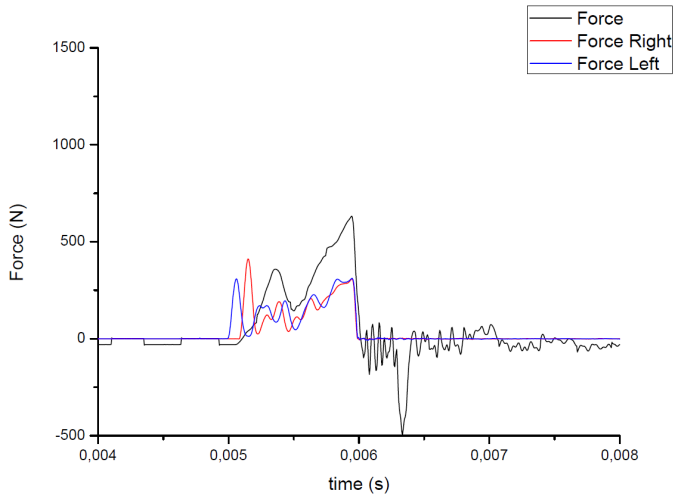

Fig. 4.12: PMMA, DEN(T). This figure reproduce a test performed with a real DEN(T) specimen and with a proper alignment tool, nonetheless there is a small delay in the impacts.

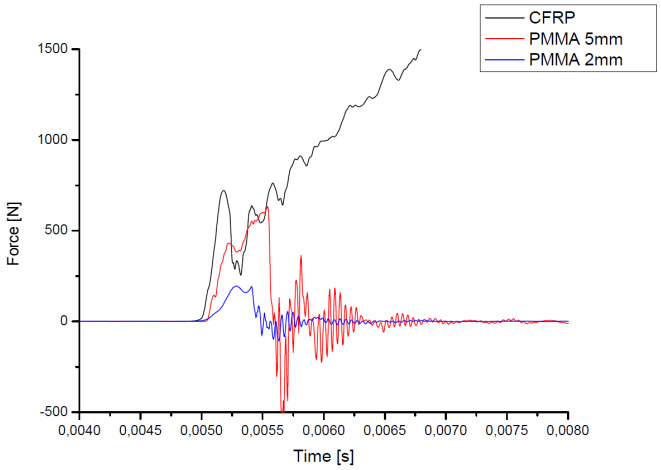

Fig. 4.13: The change of stiffness of the specimens modify the height and the duration of the initial bump demonstrating the dynamic nature of the phenomenon. In the legend the specimens are reported in order of decreasing stiffness; this can be reduced changing material and depth of notch.

4.3.3 Enschede. Tensile configuration

In this experimental section data have been recorded from specimens made of two materials, commercial PMMA and PVC, shaped as SEN(T) and DEN(T); of these kinds of specimens the main distinguishing feature is the notch depth with three different values: $a/W = 0.2$, $a/W = 0.35$ and $a/W = 0.5$. The total amount of specimens tested is about 100. The velocities chosen are 1 m/s and 2 m/s.

The discussion of test results is started here from the stiffest specimens because their behaviour s closest to what is expected. Analysing the traces it's been verified that, even with difficulty, the regression proposed by the standard can produce values for K_Q comparable to those by Visser [3]. Other than the oscillations there is a second problem that makes the regression difficult for these test results: the limiting condition for linearity is almost always violated. These tests are not valid for ISO 17281. The apparent non-linearity is induced by an unexpected dynamic behaviour during the impact of the system: in the early instants of force rise a very fast growth of F is seen and after a while oscillations become dominant and they seem to follow

a linear envelope with lower slope. This is quite clear for Figure 4.17: the two curves representing the stiffest specimens have the same rising ramp in the beginning and then they oscillate around a same mean line; frequencies are slightly different because of different stiffness. Also the weakest specimen of the three shows the same behaviour but because of a small error in alignment the behaviour is not as close as the others. For these specimens force ramps are of 0.2 and 0.28 ms in duration and reach about 500 N. Oscillation frequencies are 6.37, 4.98 and 4.17 kHZ.

From these observations it's possible to infer that the different behaviour is not because of a difference between the specimens but is surely de to the test set-up.

As for 5 mm DEN(T) specimens also for 5 mm thick SEN(T) specimens apparent non-linearity has been found. In this case the two different stages are less clear because the initial rise is much lower. It's mostly evident in Figure 4.22. As for the DEN(T) also here frequency and rise force are lower for weaker specimens.

The most problematic interpretation arises with the mostly weak specimens: the 2 mm thick specimens (both SEN(T) and DEN(T)) are so delicate that the dynamic effects cover specimen's behaviour completely and so no analysis can be done with reasonable reliability. In Figure 4.15 and 4.16 as in Figure 4.20 the test duration is so short that it results to be less then those 0.2 ms typical of the initial rising. The test cannot be used to investigate the behaviour of the material

4.3.4 Milano. Pendulum tests

The first set of experiments collected consist of both DEN(T) and SEN(T) specimens. The machine used is a pendulum. Multiple tests have been performed, 32 DEN(T) and 9 SEN(T). The sizes of the samples are all of 80 mm of length (48 mm of span length), 10 mm of width and the nominal thickness is about 2 and 5 mm. Three notch depths were used: 2, 4 and 6 mm. The velocity is 1 m/s and correspond to an energy of about 3.8 J.

Some of the recorded forces are presented in Figure 4.24, 4.25 and 4.26

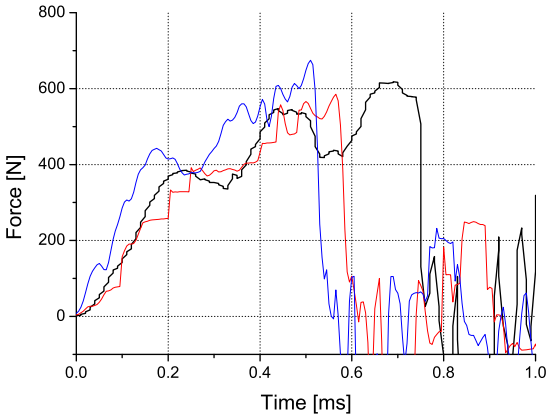

Fig. 4.14: Drop-weight test, PMMA, DEN(T), 2 mm thickness, $a/W = 0.2$.

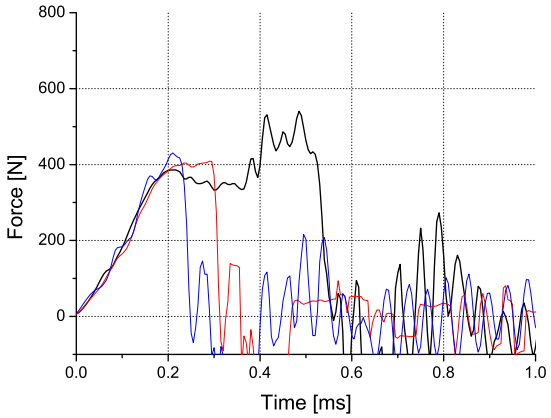

Fig. 4.15: Drop-weight test, PMMA, DEN(T). 2 mm thickness, $a/W = 0.35$.

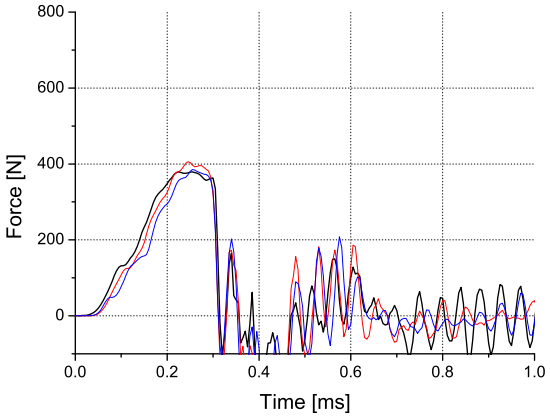

Fig. 4.16: Drop-weight test, PMMA, DEN(T). 2 mm thickness, $a/W = 0.5$.

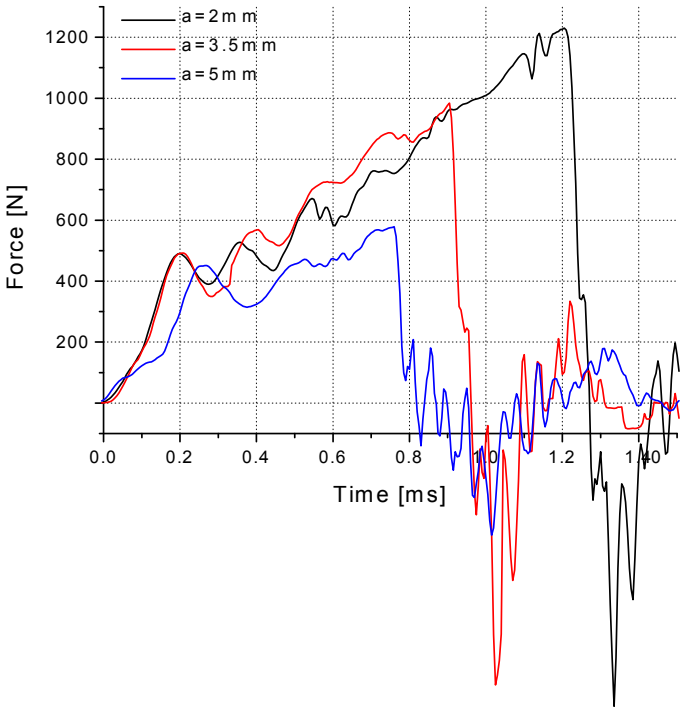

Fig. 4.17: Drop-weight test, PMMA, DEN(T). 5 mm thickness.

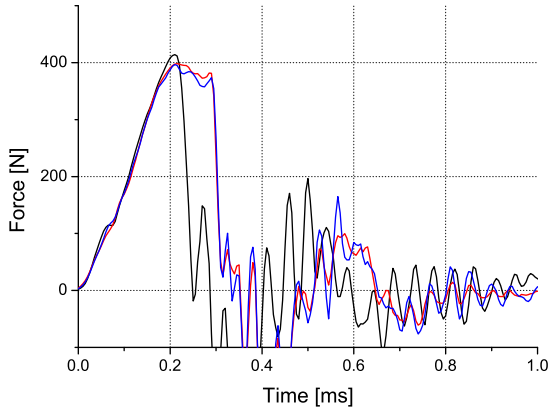

Fig. 4.18: Drop-weight test, PMMA, SEN(T), 2 mm thickness, $a/W = 0.2$.

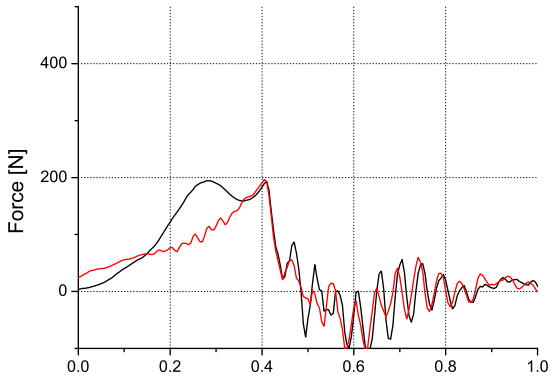

Fig. 4.19: Drop-weight test, PMMA, SEN(T), 2 mm thickness, $a/W = 0.35$.

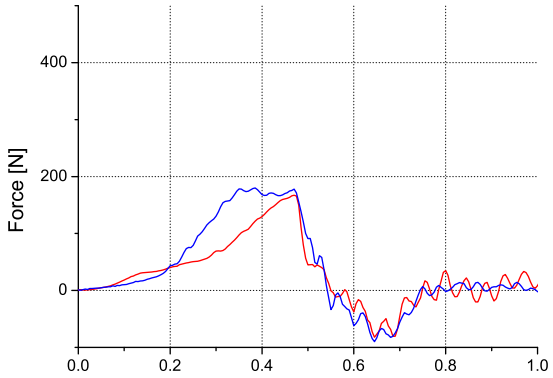

Fig. 4.20: Drop-weight test, PMMA, SEN(T), 2 mm thickness, $a/W = 0.5$.

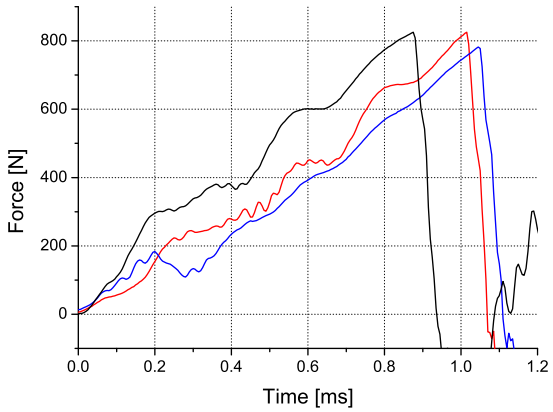

Fig. 4.21: Drop-weight test, PMMA, SEN(T), 5 mm thickness, $a/W = 0.2$.

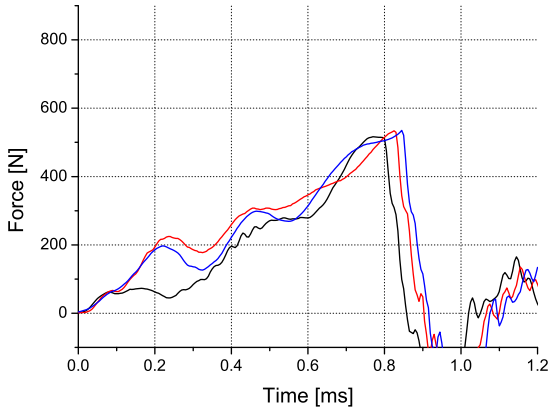

Fig. 4.22: Drop-weight test, PMMA, SEN(T), 5 mm thickness, $a/W = 0.35$.

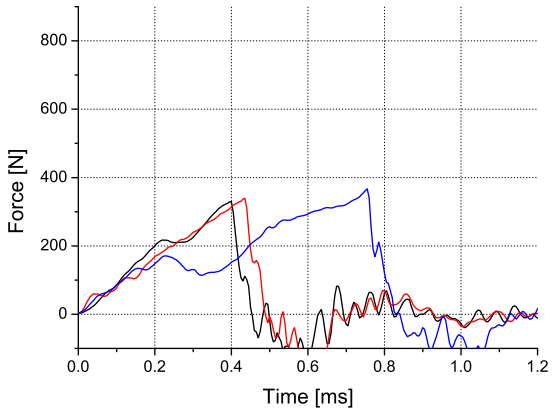

Fig. 4.23: Drop-weight test, PMMA, SEN(T), 5 mm thickness, $a/W = 0.5$.

Type	Thickness [mm]	Notch [mm]	Stiffness [N/m]	F_{th} [N]
SEN(B)	5	2	$7.9 \cdot 10^5$	213
		3.5	$5.3 \cdot 10^5$	144
		5	$3.1 \cdot 10^5$	94
SEN(T)	2	2	$1.6 \cdot 10^6$	368
		3.5	$1.3 \cdot 10^6$	205
		5	$1.2 \cdot 10^6$	113
	5	2	$3.9 \cdot 10^6$	920
		3.5	$3.3 \cdot 10^6$	514
		5	$2.3 \cdot 10^6$	282
DEN(T)	2	1	$1.6 \cdot 10^6$	632
		1.75	$1.6 \cdot 10^6$	470
		2.5	$1.5 \cdot 10^6$	377
	5	1	$4 \cdot 10^6$	1581
		1.75	$3.9 \cdot 10^6$	1174
		2.5	$3.8 \cdot 10^6$	941

Tab. 4.1: Values of specimens' stiffness calculated for various geometries and dimensions. In the last two columns are reported also the expected maximum force for and ideal case. Note that these values are good for specimens composed of PMMA with an elastic modulus $E = 2.878$ MPa at a load-rate of about $\dot{\epsilon} = 20\ s^{-1}$, corresponding to $v_{imp} = 1$ m/s.

and 4.27, 4.28 and 4.29. In preparation to experiments, estimations of the main parameters have been made resulting into the values proposed in Table 4.1. The estimation of maximum force F_{th} is done trough the calculated value of specimen's stiffness and loading rate.

In the tests performed some non-linearities are present, as shown in Figure 4.26. These are supposed to be caused by the effect of grease applied on the cross-head or, according to Ghezzi [2], due to horizontal misalignments. The maximum recorded forces are comparable to that found in experiments done with other machines and by other operators.

4.3.5 Milano. Drop dart tests

As a last term of comparison a different drop-weight machine has been used. The machine is equipped with a dart and measure the force exchanged during impact as the other tw presented. The test configuration is again 3PB. The

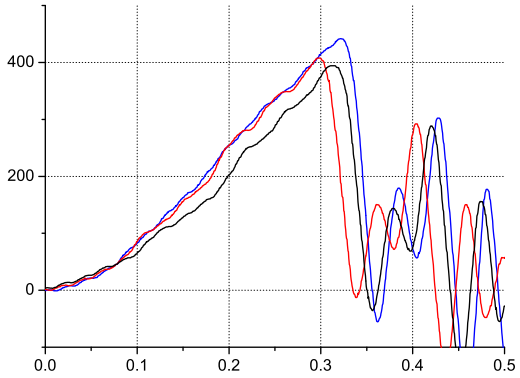

Fig. 4.24: PMMA, SEN(T), $a/W = 0.2$ and $B = 2$ mm. $v_i = 1$ m/s.

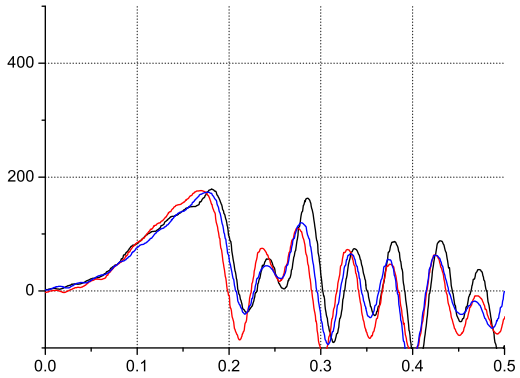

Fig. 4.25: PMMA, SEN(T), $a/W = 0.4$ and $B = 2$ mm. $v_i = 1$ m/s.

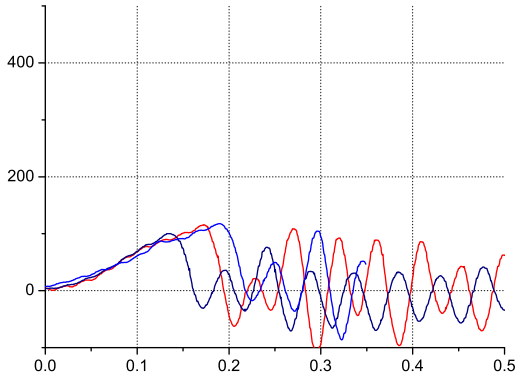

Fig. 4.26: PMMA, SEN(T), $a/W = 0.6$ and $B = 2$ mm. $v_i = 1$ m/s.

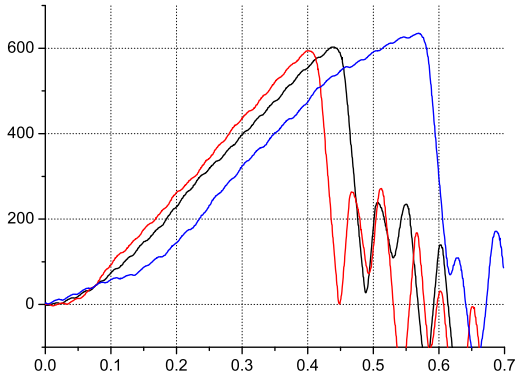

Fig. 4.27: PMMA, SEN(T), $a/W = 0.2$ $B = 5$ mm. $v_i = 1$ m/s.

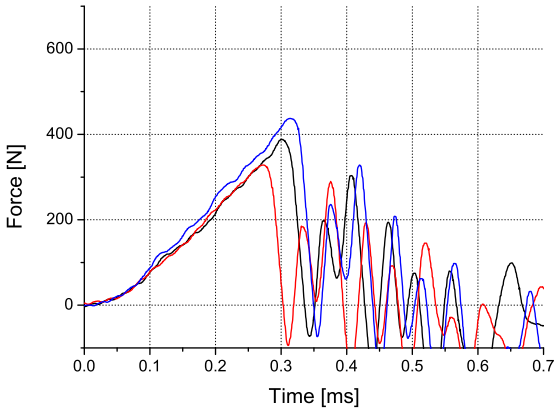

Fig. 4.28: PMMA, SEN(T), $a/W = 0.2$ $B = 5$ mm. $v_i = 1$ m/s.

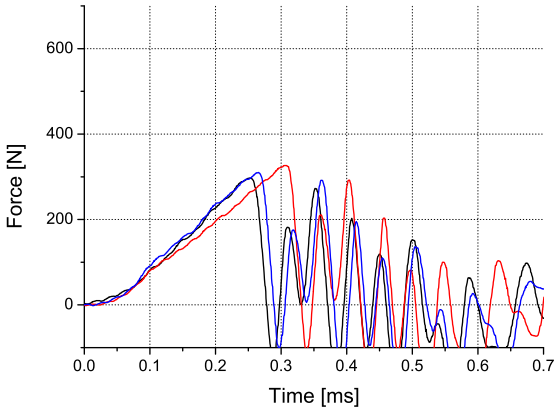

Fig. 4.29: PMMA, SEN(T), $a/W = 0.2$ $B = 5$ mm. $v_i = 1$ m/s.

tested material is again PMMA and the thickness chosen is been 5 mm.

The results presented indicate that the proposed design has to be modified to reach a better recording quality. In order to do this the source of the strong dynamic manifestations has to be understood.

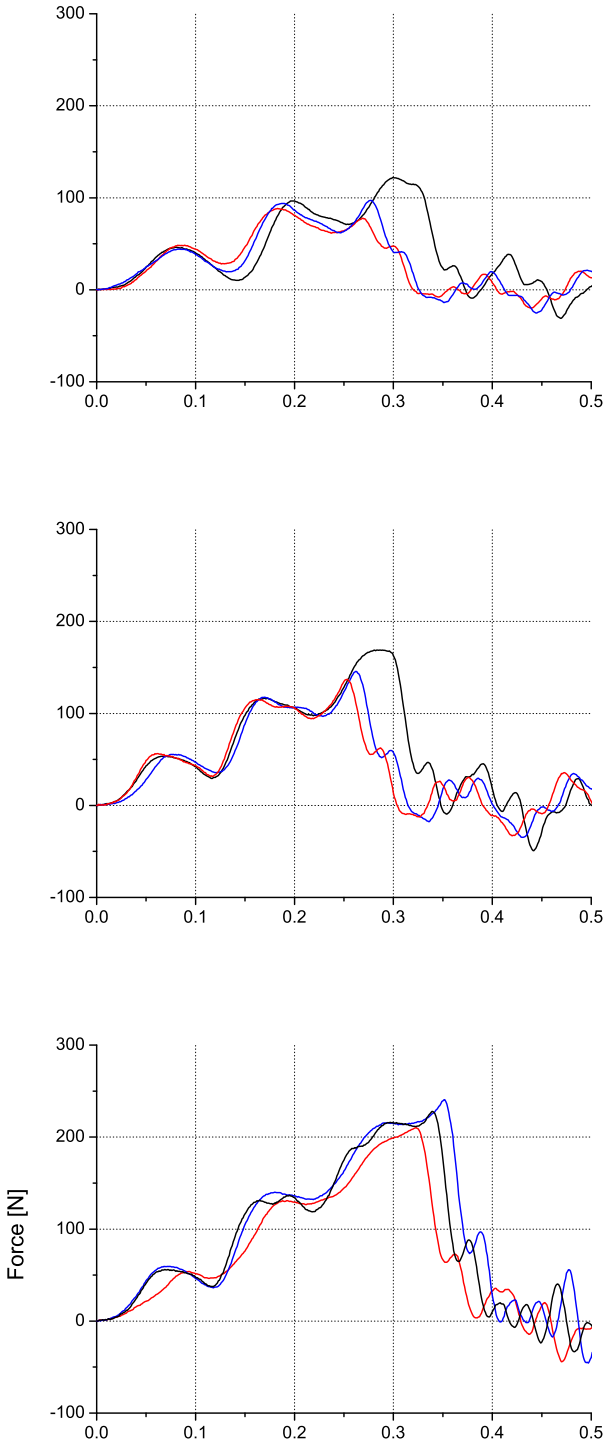

Fig. 4.30

5. ANALOGUE MODEL

The results presented in the preceding chapter alighted that the set-up is prone to transfer dynamic effects. In all the traces from the drop weight tower we can see pronounced oscillations. Regression on those force traces is less reliable because of oscillation amplitude. They can make it impossible to regress the average instantaneous force acting on the force cell.

This chapter present the effort done to identify the main causes of the unwanted response of the machine. This has been done comparing some results obtained from the pendulum in Milan and in Enschede with the output of an analogue model. This kind of models are relatively simple but if accurately prepared they can describe the behaviour of the system studied.

5.1 Model definition

The presence of fluctuations on the traces is caused by inertial effects of the elements that constitute the assembly and that connects the specimen and the transducer. This is the main problem of any dynamic test: when the time scale of an event lowers, the importance of mass and stiffness increases dramatically.

During the machine calibration some elements have been found in the set-up which are not adequate for good performance; the adequacy of the measurements can be defined in terms of force at fracture, in effects F_{max}, and oscillations amplitude, F_a. The smaller is $\frac{F_a}{F_{max}}$, the more reliable are the estimations.

To have an idea of the effect of masses and stiffnesses an analogue model composed of two springs, K_1 and K_2, and two masses, m_1 and m_2, can be used. An hypothesis is at the basis of this model: the only two components

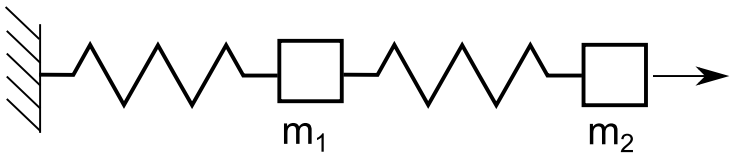

Fig. 5.1: Schematic representation of an analogue model used to understand the interaction between specimen and transducer.

of the system that have non-zero compliance are specimen and transducer (or the assembly that connect the specimen to the frame). A representation of the system is shown in Figure 5.1. The system can be simplified considering the boundary condition of constant velocity for the first mass, this is like to use a striker with a mass much higher then that of the specimen and of the clamp. Under this hypothesis the equations describing the system are these:

$$\begin{cases} \ddot{x}_1 = 0 \\ \ddot{x}_2 = \frac{K_1}{m_2} x_1 - \frac{K_1+K_2}{m_2} x_2 \end{cases} \tag{5.1}$$

where x_1 and x_2 are the displacements of the two masses. Springs' deformations are $\Delta x_1 = 1_1 - x_2$ and $\Delta x_2 = x_2$; the solution for the system has the form

$$\begin{cases} x_1 = v_{imp} t \\ x_2 = \frac{K_1 v_0}{\omega^3 m_2} \left(\omega t - sin\left(\omega t\right)\right) \end{cases} \tag{5.2}$$

with $\omega = \sqrt{\frac{K_1+K_2}{m2}}$. In Figure 5.2 the result of a simulation is shown for $v_0 = 1$ m/s, $m_2 = 0.05$ kg, $K_1 = 2.97$ kN/mm and $K_2 = 3$ kN/mm. In this simulation a stiffness K_2 much lower that K_1 has been used, this to simulate the compliance of the features that connect the load cell to the specimen. This is a more realistic choice then considering the proper stiffness of the piezo ($K_{cell} \cong 1$ MN/mm); in Figure 5.2b the simulation for the same parameters but with $K_2 = 1MN/mm$ is represented, it's clear that this is not representative of the experiment itself. This simple model shows almost what we record from the piezo but it's clear that this do not dominated by its characteristics.

In the course of the present study a small analysis to try has been performed

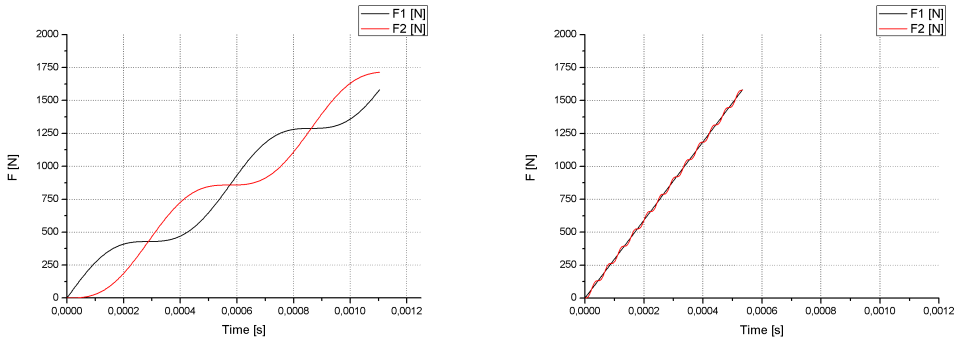

(a) (b)

Fig. 5.2: Forces acting on specimen and load-cell obtained for a two-springs model to simulate the effect of dynamic interactions between specimen and load-transducer. a) The parameters considered in this simulation are $v_0 = 1$ m/s, $m_2 = 0.05$ Kg, $k_1 = 2.97$ KN/mm and $K_2 = 3$ KN/mm. The most notable things are that $t_f = 1.1$ ms and the difference of F_Q evaluated on F_2 and the theoretical F_{max}: $\triangle F = 130$ N. b) Same simulation but considering the stiffness of the load-transducer ($K_2 = K_{cell} \cong 1$ MN/mm).

to uncouple the load-washer and the fixture that surrounds it. To do this a three springs and three masses analogue model has been used. In this case no closed form solution has been calculated but a numeric integration was used. In Figure 5.3 the output from such a model is shown. It's possible to see that the load cell follows the behaviour of the element that precedes it and tends to remain close to it as long as the difference in stiffness is high (in favour to the piezo). In the first case the force trace from the specimen is almost the average of the cell's one; in the second the difference between the one from the fixture and that from the cell is vanishing. The consequence of this is that the signal coming from the piezo is dominated by the interaction of the specimen with the fixture; the reason for this is the huge difference in compliance of the transducer from the whole fixture (should be noted that the fixture is composed by a series of elements that contains also the transducer itself). This is a confirmation of the choice done in the two-springs model where a stiffness $K_2 = 3KN/m$ has been used.

From this considerations it's possible to consider the two-spring model as reliable as the three-springs one is. This is not guarantee for precision but it

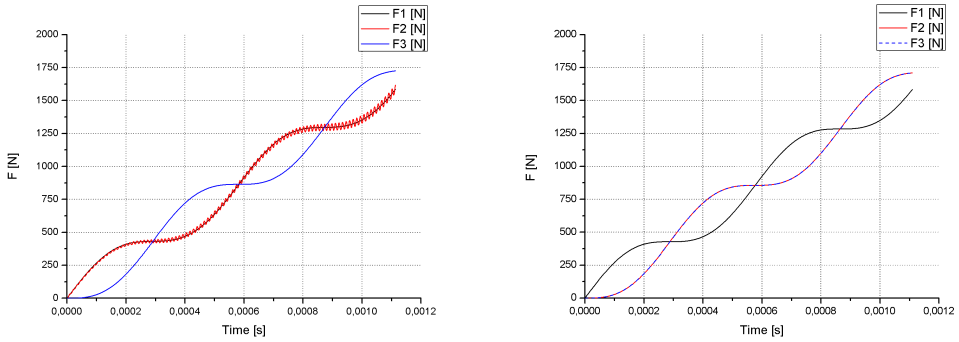

(a) (b)

Fig. 5.3: A model composed of three springs and three masses has been used to check the effect of the sample and of the fixture on the signal recorded for the load washer. a) The parameters used are: $v_0 = 1m/s$, $m_2 = 0.05Kg$, $m_3 = 0.001Kg$, $k_1 = 2.97KN/mm$, $K_2 = 1MN/mm$ and $K_3 = 3KN/mm$. b) The cell is in the second position.

permits the use of a very simple model.

5.2 Assessment of machine's parameter

In the previous section simulations for the model have been shown and some parameters have been already defined, to have a proper estimation of them we present them again in more detail. The two couples spring-mass represent the behaviour of the specimen itself (designated with the subscript "1") and of the assembly that connect the specimen with the frame. This last is composed by the *fixed clamp*, the *pre-compression screw*, the *piezo* and the *hinge*. The assembly is a complex system that has its own behaviour but this would require a wide study itself and it's accounted to affect the minor effects that appear in the experimental records. Even if this can't be described only as a *series* of elements its global behaviour will be supposed as dominated by the weakest components in it. Out of the four elements mentioned, the most compliant seems to be the skew for it's slenderness. In Table 5.1 some values, estimated with simple calculations for the stiffness (definition for static conditions is used), are reported. The apparent stiffness

that will be measured in the tests performed to characterize the machine have to be used in the model to check whether or not the global compliance of the fixture is the sum of compliances or not.

$$\frac{1}{K_2} = C_2 = C_{fixture} = \sum_i C_i \tag{5.3}$$

The estimation of the specimen's stiffness has been presented before; refer to Table 4.1 for gross values of the parameter for various dimensions and geometries of the specimens.

The evaluation of the parameter m_2 is much simpler since it's the sum of the masses of the components:

$$m_{tot} = \sum_i m_i \tag{5.4}$$

The evaluation of the stiffness of the machine can be performed by running

Element	Stiffness	Mass
Clamp	10 MN/mm	10 g
Skew	200 KN/mm	5 g
Piezo	1 MN/mm	1 g
Hinge	0.5 MN/mm	50 g

Tab. 5.1: Stiffnesses and masses for the elements that constitute the fixture affecting the load-cell and so those which "filter" the force acting on the specimen.

an impact test on a sample of controlled compliance and subtracting that of the specimen, $K_s = K_1$ from the one evaluated from the force trace.

$$\frac{1}{K_{ap}} = C_{pa} = C_1 + C_2 \tag{5.5}$$

so we can invert the relation and say that

$$K_2 = \frac{1}{C_{ap} - C_1} \tag{5.6}$$

where K_{ap} is the apparent stiffness, that measured on the curve $F - \delta$. The precision of the measure of K_2 is strongly affected by the difference between the measure of the apparent compliance and that of the specimen. A manner to keep the sensitivity at an acceptable level is to make this difference as big as possible: the stiffness of the machine have been identified, in previous tests, to be about 5 kN/mm so new specimen's stiffness should be much higher. For this reason and due to the simplicity of machining Aluminium the evaluation of machine's stiffness has been performed with an un-notched specimen with the same dimensions of the polymeric ones. Its characteristics are reported in Table 5.2. With such a difference in the stiffness we clearly un couple the

Material	Aluminum
E Modulus	72 GPa
Width	9.38 mm
Length	48 mm
Height	5.09 mm
Stiffness	72.6 kN/mm

Tab. 5.2: properties of the Aluminum specimen used for machine's characterization.

effect of machine's structure from that of the specimen and we can have an insight of the behaviour of the tester.

5.2.1 Measures on pendulum - Milan

In this section the few traces recorded with the pendulum using an Aluminum specimen are shown: the test are performed at moderately low speed to avoid overloading of the machine; the speed ranges from 0.2 m/s to 0.5 m/s, with the pendulum is quite easy to set such low speeds with precision because of the almost linear dependence of v_0 form the angle. For the pendulum the apparent stiffnesses of the machine itself, measured on the traces, result to have an average $K = 6.30 \pm 0.87$ kN/mm. This stiffness is of the same order of magnitude of the PMMA specimens ($\cong 3$ kN/mm).

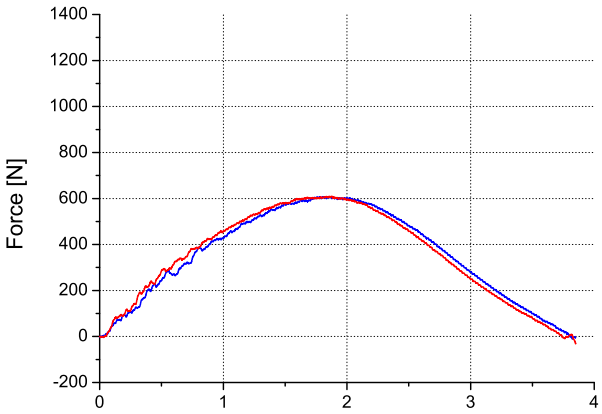

Fig. 5.4: Force traces: recorded during impact at 0.2 m/s with the pendulum machine. In the test a grease layer of 0.1 mm thickness has been used to improve the readability of thee result. The specimen used is an un-notched one made of Aluminum.

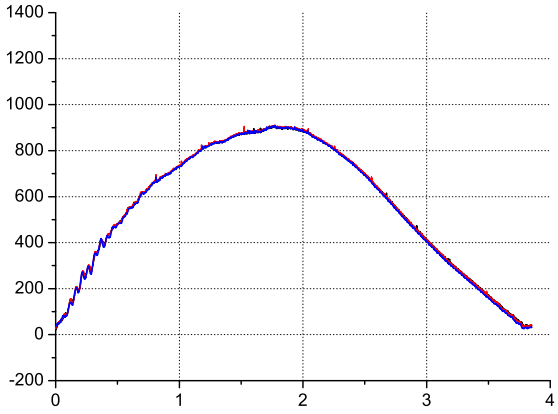

Fig. 5.5: As the preceding diagram three test are shown in the image. Represent the forces exchanged during an impact at 0.35 m/s.

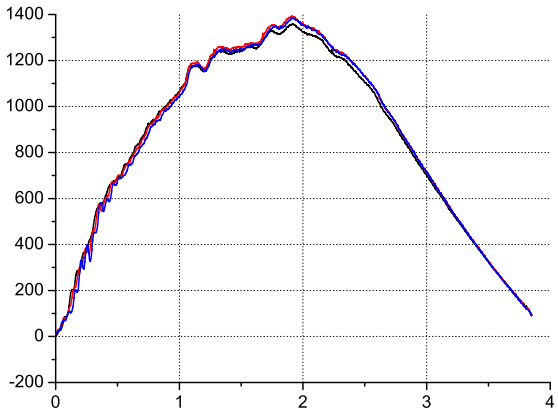

Fig. 5.6: As the preceding diagram three test are shown in the image. Represent the forces exchanged during an impact at 0.5 m/s.

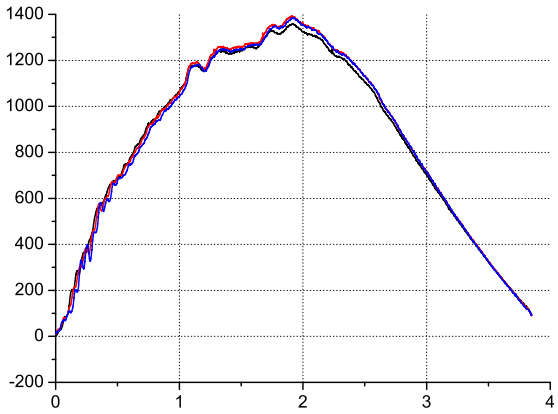

Fig. 5.7: Impacts' recorded traces from the drop-tower. Here are shown only those related to the impacts at 0.5 m/s because the locking system for this machine is interfering in the earliest instants of the fall and for low velocities the drop-heigh is so slow that the test is no more reliable.

5.2.2 Measures on drop weight tower - Enschede

The same kind of measure described as before has been done on the drop tower. The recorded traces show a behaviour that is not confirming the hypothesis made before: with the PMMA and PVC specimens the oscillations appeared to be not negligible, too wide to allow a proper identification of the crack initiation force, with Al it seems that oscillations are smaller but it's just the effect of different steepness of the force trace.

In Figure 5.7 some of the recorded impacts are shown. From this image is immediately recognizable that the behaviour of the machine is not what expected. This difference has been also confirmed by the calculations.

Curves show a stiffness $K = 1.84 \pm 0.23$ kN/mm. From these data we can calculate the apparent stiffness of the set-up, as done for the pendulum. The resulting stiffness has an average of $K_{eff} = 4.10 \pm 0.54$ KN/mm.

What appears from the numbers presented is that the stiffness shown by both the machines is within the same order of magnitude demonstrating that the design is not weak from this perspective. The reason that explain the difference between the tests performed should hence be connected to some other aspects of the test.

6. CONCLUSIONS

Impact event are recognized to be one of the most critical conditions of loading and so a proper knowledge of the behaviour of material in this sense is important. Some standards are available to measure toughness also for visco-elastic materials at low speed (less then 1 m/s) but it's still missing a proper, simple and cheap technique to measure this parameter at high impact speeds. Mainly the problems are related to uncouple dynamic effects in the recorded force from the actual force acting at the failure point. Better results can be obtained using tensile configuration. It is necessary to confirm this result and so a new set-up has been designed. The presented set-up was designed, produced and used to perform various tests. During the design attention has been dedicated to mass, stiffness and force transmission: the problem of loading a specimen out from its inertial axis is that this is loaded in non-pure tensile condition.

A set of specimens was tested to obtain some information on the behaviour of the machine. The considered configurations have been: SEN(B), SEN(T) and DEN(T). They are characterized for two nominal thickness (2 and 5 mm). Principally the interest of the present work was on DEN(T) specimens because they are symmetric, the remaining two have been used to check results using very well known specimens, for which in literature is present quite some informations.

The results obtained show that the behaviour of the new machine is very different from that of the former one (a pendulum). Stronger oscillations are recorded and sometimes these completely hide the information of interest, especially for weak specimen.

This problem has been studied and an hypothesis have been formulated: the stiffness of the machine, or of part of it is too low. This seemed reasonable

because lower stiffness's often are related with wider and longer vibrations. A very simple spring-mass model, composed of two spring, have been used to check the hypothesis. An estimation of the stiffness has been obtained both for the new machine and for the pendulum used before. The stiffness has been measured using an Aluminum sample of well known stiffness and calculating the slope of the F curve. The resulting stiffness's are not so different: 6.3 kN/mm for the pendulum and 4.1 for the drop-tower. This small difference is not sufficient to justify the large difference and so a more detailed study should be performed to check its causes. Some doubts lay on the behaviour of the most critical parts: the hammer and the fixed clamp. The first is quite long and therefore is compliant, the second is a complex assembly of components that interact with the specimen and can introduce noise on the measure. The complexity of the clamping apparatus can hide some aspects not considered in the design.

The new set-up, at the present, is not to be considered a reliable tool to measure toughness of very weak specimen (they must show a force at fracture $F_{frac} >= 200$ N). Being far from a completion the study of this machine can give an insight for further developments: the different behaviour form the pendulum suggest a difference in some design detail. As said the main doughs lie on the screw that compresses the transducer, in fact as shown in the last chapter the best results in these kinds of measures are obtained using a loading and measuring system as stiff as possible. At this point is necessary to revise the design to improve rejection to oscillations; to improve machine's behaviour should be evaluated the use of a bigger transducer and studied in detail the dynamic interaction of it with the compression screw and the fixed clamp. In the future studies should be considered also the effect of the hinge: in the present case a rod-end hinge was chosen, this has a brass ring to reduce friction but this showed to be too soft.

APPENDIX

A. SENSITIVITY

It's a well known fact that in experiments errors are unavoidable. Their presence is manifest in any kind of experiment and some times is a real problem, it's fundamental to understand how to keep them in consideration and estimate them. Normally the first approach is to describe the randomness of the measure through recording on multiple measures: a proper measure is composed of a *mean value* and its *variability*. The definition of mean value is well known and in case of an array of data points is

$$\bar{x} = \frac{\sum_{n=1}^{N} x_n}{N} \tag{A.1}$$

We are also interested to describe our uncertainty of the measure, to define its reliability. The proper parameter for this is the variability of the *measure*, so the variability of the *average value* that is the best estimation of the measure itself. Then, the expression of measure's dispersion is $\sigma^2(\bar{x})$, not $\sigma^2(x)$; the last describes the variability of the phenomenon itself, not of the measure. Clearly $\sigma^2(\bar{x})$ and $\sigma^2(x)$ are correlated but they describe two different aspects of the statistical phenomenon. The expression of the variability of the average values can be inferred by the definition:

$$\sigma^2(\bar{x}) = \sigma^2\left(\frac{\sum_{n=1}^{N} x_n}{N}\right) = \frac{\sum_{n=1}^{N} \sigma^2(x_n)}{N^2} = \frac{\sigma^2(x)}{N} = \frac{s^2(x)}{N} \tag{A.2}$$

and we can define the uncertainty as $u(x) = \frac{s(\bar{x})}{\sqrt{N}}$ and the measure can be correctly expressed as $x = \bar{x} \pm \frac{s(\bar{x})}{\sqrt{N}}$. Note that the estimation of $\sigma^2(x)$ from a data array has the form of $s^2(x) = \sum_{n=1}^{N} \frac{(x-\bar{x})^2}{N}$. The most critical

measure has been identified as that of specimen dimensions: the slope of the shape-factor curve in many cases is quite high. The slope has the effect of *amplifying* the variability of the data introduced: if we have high precision on the measure of a and w then the error can be contained, on the contrary if the variability is too big the data have no reliability on the measure and so this last has no meaning. The first thing to do is to give an estimation of an acceptable final variability and from that to estimate the adequate resolution on the measure of specimen dimensions. The best thing to do to make this is to start comparing the shape factor expressions, these are reported in Table A.1. Refer to Figure A.4 to have a comparison of the different shape factors; in Figure A.5 are represented the derivatives (with respect to $x = \frac{a}{w}$) of shape factors in the three cases. For the estimation of the maximum acceptable variability of the parameter $\frac{a}{w}$ we can consider the definition of sensitivity:

$$S(a/w) = \frac{\partial K_Q}{\partial(a/w)} = \frac{F_Q\sqrt{\pi}}{B\sqrt{w}}\left(\frac{f}{2\sqrt{a/w}} + \sqrt{a/w}f'\right) \quad \text{(A.3)}$$

and we can say that

$$S(a/w) = K_Q\left(\frac{w}{2a} + \frac{f'}{f}\right) = K_Q \cdot z(a/w) \quad \text{(A.4)}$$

Considering a linearisation around the measure point we can say

$$K(a/w) \sim K_Q(a_0/w_0) \pm u_{K_Q} \sim K_Q(a_0/w_0) \pm S(a_0/w_0) \cdot u_{\frac{a}{w}} \quad \text{(A.5)}$$

From this last equation we find the relation between uncertainty on a/w and on K_Q; if we suppose acceptable a uncertainty of $u_{K_Q} = 0.1MPa\sqrt{m}$, we need at least an uncertainty on a/w of about 0.038 mm[1]. Typical values for the three specimens are reported in Table A.2. This does not take into account uncertainty on the force, only the effect of the shape factor so the

[1] The value reported of uncertainty of the ratio a/w is the one corresponding to the worst case so that it will result adequate for any situation. The worst case is that of SEN(B) with a notch depth of $a/w = 0.6$

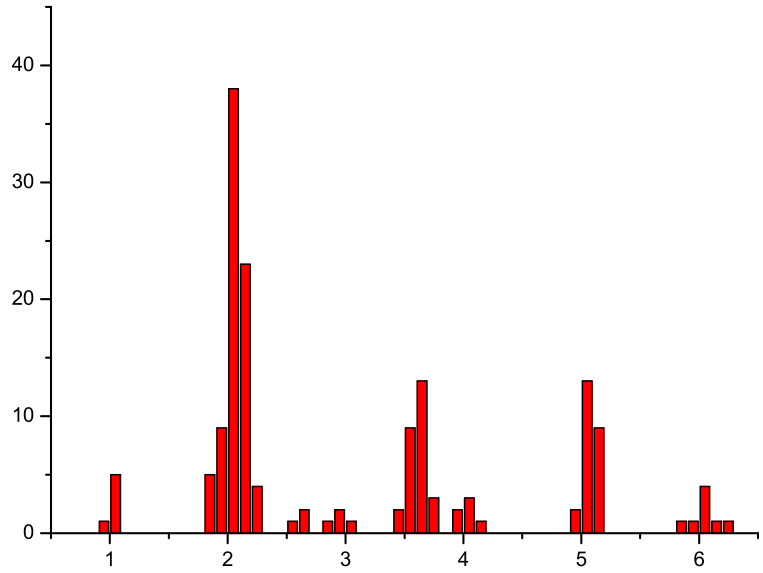

Fig. A.1: Distribution of the measured values of a for the whole set of specimens. Since to different values of a correspond a different number of specimens the hight of peaks can't be compared with that of other; on the opposite it's possible with the width (variability), especially for those with a substantial number of measure. The mean values are 1 mm, 1.75 mm, 2 mm, 2.5 mm, 3 mm, 4 mm and 5 mm

variability will be higher in the real cases. In Figure A.1 are shown some box plots about the measures of the three characteristic sizes of the specimens, the data proposed refer to the measures taken for the 3PB tests performed at the University of Twente.

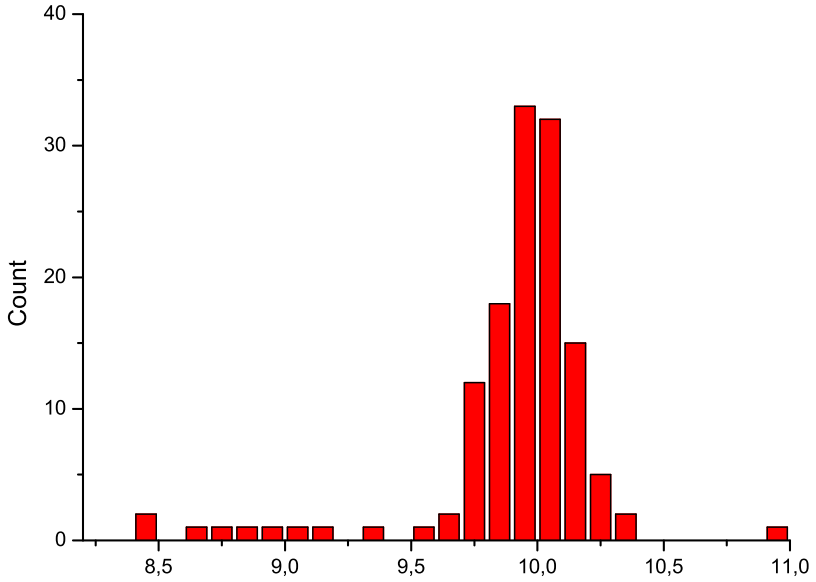

Fig. A.2: The effective value of uncertainty as defined in Section 3.1.1

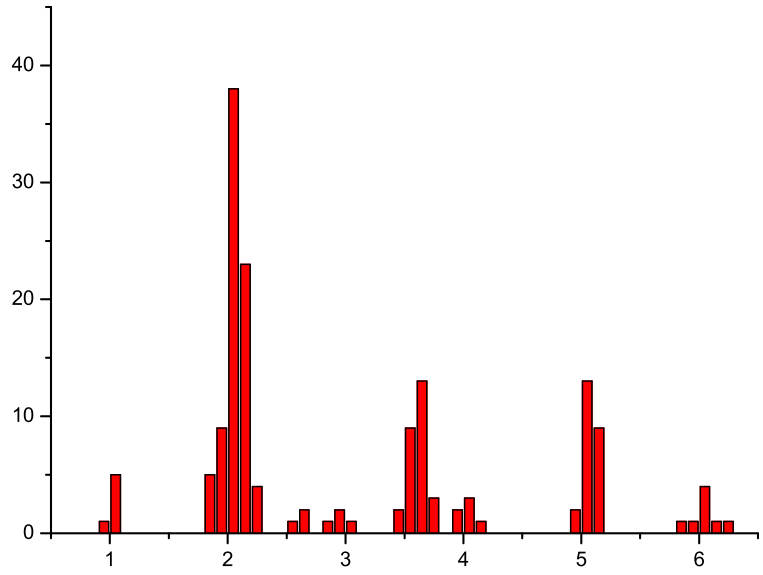

Fig. A.3: The distribution of the averages is not clear so it can be supposed Gaussian, no indication have been found of particular structures in data distribution.

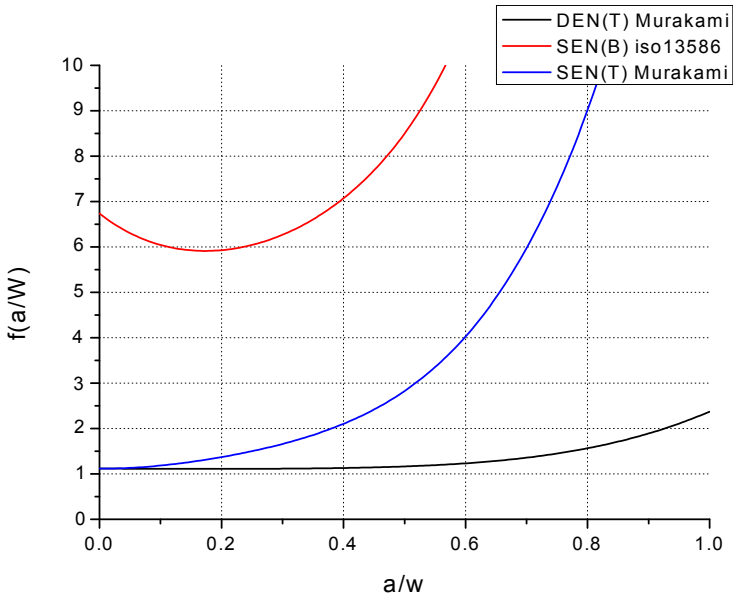

Fig. A.4: The difference between the three shape factors for SEN(B), SEN(T) and DEN(T) is clear in the plot.

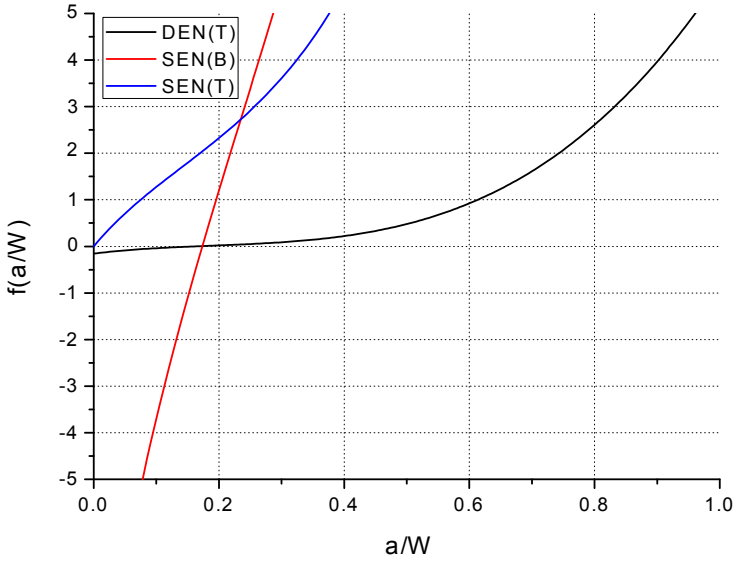

Fig. A.5: In this figure are presented the derivatives for the three types of shape factors. The most important aspect that emerges form this is that the instantaneous value of those changes a lot. In case of SEN(B) and SEN(T) is quickly very high. Should be noted that the value of sensitivity is proportional to that of derivative.

Tab. A.1: DEN(T) shape factors.

	Shape Factor	*Source*	*constrains*
DEN(T)	$1.12 + 0.2\frac{a}{w} - 1.2\left(\frac{a}{w}\right)^2 + 1.93\left(\frac{a}{w}\right)^3$	Bowie	$\frac{l}{w} = 6,\ \frac{a}{w} < 0.7$
	$\frac{1.12-0.56\frac{a}{w}-0.015\left(\frac{a}{w}\right)^2+0.091\left(\frac{a}{w}\right)^3}{\sqrt{1-\frac{a}{w}}}$	Benthem, Koiter	
	$1.122 - 0.154\frac{a}{w} + 0.807\left(\frac{a}{w}\right)^2 - 1.894\left(\frac{a}{w}\right)^3 + 2.494\left(\frac{a}{w}\right)^4$	Nisitami	$\frac{a}{w} < 0.8$
SEN(T)	$1.12-0.23\frac{a}{w}+10.6\left(\frac{a}{w}\right)^2-21.7\left(\frac{a}{w}\right)^3+30.4\left(\frac{a}{w}\right)^4$	Brown, Srawley	$\frac{l}{w} = 6,\ \frac{a}{w} < 0.7$
	$\frac{1+3\frac{a}{w}}{2\sqrt{\pi\frac{a}{w}}\left(1-\frac{a}{w}\right)^{3/2}}$	Orange	$l/w > 2,\ a/w > 0.3$
	$\frac{1.988}{\sqrt{\pi}}\frac{0.0268\left(0.4271+\frac{a}{w}\right)^{-2.739}+0.2651\frac{a}{w}+0.7248}{\left(1-\frac{a}{w}\right)3/2}$	Fett Munz	
SEN(B)	$\frac{6}{\sqrt{\pi}}\frac{1.99-\frac{a}{w}\left(1-\frac{a}{w}\right)\left(2.15-3.93\frac{a}{w}+2.7\left(\frac{a}{w}\right)^2\right)}{\left(1+2\frac{a}{w}\right)\left(1-\frac{a}{w}\right)^{3/2}}$	ISO13586	

Tab. A.2: Sensitivity

a/w	*SEN(B)*	*SEN(T)*	*DEN(T)*
0.1	8.38459	2, 2982	1.74421
0.2	7, 16659	2, 58567	1, 25091
0.3	8, 78607	3, 44148	1, 0666
0.4	12, 37259	5, 18147	1, 0332
0.5	19, 06679	8, 5209	1, 16204
0.6	32, 77373	14, 39488	1, 5109
0.7	66, 74278	23, 90602	2, 1607

B. SENSITIVITY OF IMPACT VELOCITY FROM FALLING HIGH

The regulation of the heigh of drop is important as it defines the impact velocity but the sensitivity from the height varies with speed; to have an idea of what is the sensitivity from this parameter let's consider negligible the friction effects of the bushing with the rails and of viscous motion in air: in this situation we can use the energy conservation and say that

$$v = \sqrt{2gh} \tag{B.1}$$

where h is the vertical displacement and g is the gravitational acceleration. From this we can see, as exposed in Table B.1, that for very low velocities small errors in the positioning cause wider changes in the impact velocity. In case of tests performed at $0.5m/s$ an error of positioning of $1mm$ correspond to a difference of velocity of about 4% where for the case of test at $3m/s$ the change due to the same error is of about 0.1%.

Tab. B.1: Velocities and sensitivity form the height

$Velocity[m/s]$	$Height[mm]$	$Sensitivity[1/s]$
0.2	2	46.4
0.5	12.7	19.7
1	51	9.8
1.5	115	6.5
2	204	4.9
2.5	319	3.9
3	459	3.3

C. STIFFNESS MODEL

Supposing the quasi-static solution applicable to the present case F_{max} is defined equating the instantaneous toughness to the known value:

$$K_{Ic} = \frac{F_{max}}{BW}\sqrt{\pi a} f\left(\frac{a}{W}\right) \tag{C.1}$$

For the estimation of the time to fracture the value of specimen's stiffness is needed. In the three-point bending configuration this is the bending stiffness; for non-notched specimens this can be calculated with the formula

$$S_{bend} = \frac{4BW^3E'}{L^3} \tag{C.2}$$

but for specimens with a notch a correction should be applied. The actual value of the stiffness can be estimated recalling a relation true for linear elastic fracture mechanics:

$$G_{Ic} = \frac{F}{2B}\frac{\partial C}{\partial a} = \frac{K_{Ic}^2}{E'} = \frac{\left(\frac{F\sqrt{\pi a}}{BW} f\left(\frac{a}{W}\right)\right)^2}{E'} \tag{C.3}$$

so that we can say

$$\int_{C_0}^{C_a} dC = \frac{2\pi}{BE'}\int_0^a \frac{a}{W} f^2\left(\frac{a}{W}\right) d\left(\frac{a}{W}\right) \tag{C.4}$$

$$C_a = C_0 + \frac{2\pi}{BE'}\int_0^a \frac{a}{W} f^2\left(\frac{a}{W}\right) d\left(\frac{a}{W}\right) \tag{C.5}$$

C_0 is the initial compliance, C_a that for a notched specimen and E' is the effective modulus. Finally the stiffness

$$S_a = C_a^{-1} \tag{C.6}$$

where Ka is the stiffness for a specimen with a notch depth of a. Once the stiffness is known the time to fracture is calculated considering the impact velocity v_i, the length of the specimen L and F_{max}:

$$F_{max} = K_a v_i t_{frac} \tag{C.7}$$

BIBLIOGRAPHY

[1] S. Draghi Andrea Pavan. Furthe experimental analysis of the dynamic effects occurring in three-point bending fracture testing at moderately high loading rate (1 m/s) and their simulation using an ad hoc mass-spring-dashpot model. 2000.

[2] M. Ghezzi. Analisi sperimentale e modellazione della prova di frattura per impatto a trazione su materiali polimerici. Master's thesis, 2003.

[3] H.A. Visser, F. Caimmi, and A. Pavan. Characterising the fracture toughness of polymers at a high rate of loading with use of instrumented tensile impact testing. *Engineering Fracture Mechanics*, 2012.

[4] E. Bayraktara, D. Kaplan, F. Schmidt, H. Paqueton, and M. Grumbach. State of art of impact tensile test (itt): Its historical development as a simulated crash test of industrial materials and presentation of new "ductile/brittle" transition diagrams. *Journal of materials processing technology*, 204:313–326, 2008.

[5] K. Ravi-Chandar and W. G. Knauss. An experimental investigation into dynamic fracture: I. crack initiation and arrest. *International Journal of Fracture*, 25:247–262, 1984.

[6] K. Ravi-Chandar and W. G. Knauss. An experimental investigation into dynamic fracture: Il. microstructural aspects. *International Journal of Fracture*, 26:65–80, 1984.

[7] K. Ravi-Chandar and W. G. Knauss. An experimental investigation into dynamic fracture: Iii on steady-state crack propagation an d crack

branching. *International Journal of Fracture*, 26:141–154, 1984.

[8] K. Ravi-Chandar and W. G. Knauss. An experimental investigation into dynamic fracture: Iv. on the interaction of stress waves with propagating cracks. *International Journal of Fracture*, 26:189–200, 1984.

[9] K. Arakawa and T. Mada. Unsteady dynamic crack propagation in a brittle polymer. *Experimental Mechanics*, 47:609–615, 2007.

[10] K. Ravi-Chandar. *Dynamic fracture*. Elsevier, 2004.

[11] D. P. Rooke and D. J. Cartwright. *Compendium of stress intensity factors*. 1976.

[12] ISO. Plastics — determination of tensile-impact strength. Iso 8256.

[13] ISO. Plastics - determination of fracture toughness (g_iC and k_iC)- linear elastic fracture mechanics (lefm) approach. Iso 13586.

[14] ISO. Plastics - determination of fracture toughness (gic and kic) at moderately high loading rates (1 ms). Iso 17281.

[15] G. Aggag and K. Takahashi. Study of oscillation signals in instrumented charpy impact testing. *Polymer Engineering and Science*, 36(number):2260–2266, 1996.

[16] György Vörös Béla Pukanszky Szabolcs Molnàr, Akos Bezerédi. Damping of dynamic effects with elastomers in instrumented impact testing. *International Journal of Fracture*, 109:153–168, 2001.

[17] Wang Xi. A mathematical treatment for impact test. *Engineering Fracture Mechanics*, 52(2):199–204, 1995.

[18] E. R. Marur, K.R.Y. Simha, and P.S. Nair. Dynamic analysis of three point bend specimens under impact. *International Journalof-Fracture*, 68:261–273,, 1994.

[19] Valeria Pettarin, Patricia Frontini, Gulliermo Eliçabe, Marta Rink, and Andrea Pavan. Inverse analysis of impact test data: Experimental study on polymeric materials displaying brittle behaviour. *Mechanics of Time-Dependent Materials*, 8:269–288, 2004.

[20] V. Pattarin, P. Frontini, and G. Eliçabe. Inverse method for analysing instrumented impaact tests of polymers. *Fracture of Polymers, Composites and Adhesives II*, pages 265–276, 2003.

[21] S. Sahraoui and J. L. Lataillade. Dynamic effects during instrumented impact testing. *Engineering Frocfure Mechanics*, 36(6):1013–1019, 1990.

[22] J.F. Kalthoff, S. Winkler, and W. Böhme. A novel procedure for measuring the impcat fracture toughness k with pre-cracked charpy's specimens. *Journal De Physique*, 46(8):179–186.

[23] W. Böhme. Dynamic key-curve for brittle fracture impact tests and establishment of transition time. *Fracture Mechanics: twenty-first symposium*, ASTM SPT 1047:144–156, 1990.

[24] S. K. Khanna and A. Shukla. On the use of strain gages in dynamic fracture mechanics. *Engineering Fracture Mechanics*, 51(6):933–948, 1995.

[25] T. Lorriot. Specimen loading determined by displacement measurement in instrumented charpy impact test. *Engineering Fracture Mechanics*, 65:703–713, 2000.

[26] Levend Parnas and Ömer Bilir. Strain gage method for measurement of opening mode stress intensity factor. *Engineering Fracture Mechanics*, 55(3):485–492, 1996.

[27] P. Landrein, T. Lorriot, and L. Guillaumat. Influence of some test parameters on specimen loading determination in instumented charpy impact tests. *WEngineering Fracture Mechanics*, 68:1631–1645, 2001.